Title

Excitation Spillover from PSII to PSI Measured in Leaves at 77K

Running Title

Spillover from PSII to PSI in Leaves

Corresponding Author

Ichiro Terashima

Institute of Molecular Biology, College of Life Sciences,

National Chung Hsing University,

145 Xingda Rd., South Dist., Taichung City 40227, Taiwan

E-mail: terashimaichiro@nchu.edu.tw, terashimaichiro6@gmail.com

Subject Areas

(5) Photosynthesis, Respiration and Bioenergetics

(2) Environmental and Stress Responses

Number of black and white figures:5

Number of color figures:3

Number of tables: 3

Supplementary materials: two texts, 2 tables, and 10 figures.

Title

Excitation Spillover from PSII to PSI in Leaves at 77K

Running Title

Spillover from PSII to PSI in Leaves

Names and addresses of authors

Ichiro Terashima[1,2,5*], Riichi Oguchi[1,6], Kimie Atsuzawa[3], Yasuko Kaneko[4] and Masaru Kono[1,7*]

[1]Department of Biological Sciences, School of Science, The University of Tokyo, Tokyo, 113-0033, Japan

[2]Institute of Sustainable Agro-ecosystem Services, Graduate School of Agricultural and Life Sciences, The University of Tokyo. Nishi-Tokyo 188-0002, Japan

[3]Comprehensive Analysis Center for Science, Saitama University, Saitama, 338-8570, Japan

[4]Department of Natural Science, Faculty of Education, Saitama University, 338-8570, Japan

Present addresses

[5]Institute of Molecular Biology, College of Life Sciences, National Chung Hsing University, Taichung City 40227, Taiwan

[6]Botanical Gardens, Osaka Metropolitan University, Katano 576-0004, Japan

[7]Astrobiology Center, National Institutes of Natural Sciences, Mitaka 181-8588, Japan

*Corresponding authors

Ichiro Terashima (terashimaichiro@nchu.edu.tw, terashimaichiro6@gmail.com)

Masaru Kono (konom07@bs.s.u-tokyo.ac.jp)

ABSTRACT

Heterogeneous distribution of PSI and PSII in thick grana in shade chloroplasts is argued to hinder spillover of chlorophyll excitations from PSII to PSI. To examine this dogma, we measured fluorescence induction at 77K at 690 nm (PSII) and 760 nm (mainly PSI) in the leaf discs of *Spinacia oleracea*, *Cucumis sativus* and shade tolerant *Alocasia odora*, grown at high and low light, and quantified their spillover capacities. PSI fluorescence (FI) consists of the intrinsic PSI fluorescence ($F\mathrm{I}_{\alpha}$) and fluorescence caused by excitations spilt over from PSII ($F\mathrm{I}_{\beta}$). When FI *and* FII parameters between State 1 and State 2, induced by weak far-red and blue light, were compared, PSII maximum fluorescence ($F\mathrm{II}_{m}$) and $F\mathrm{I}_{\beta}$ were greater, and $F\mathrm{I}_{\alpha}$ was smaller in State 1 and thereby the spillover ratio, $F\mathrm{I}_{\beta}/(F\mathrm{I}_{\alpha}+F\mathrm{I}_{\beta})$ or $F\mathrm{I}_{\beta}/F\mathrm{I}_{m}$, was greater in State 1. Since the leftover $F\mathrm{II}_{m}$ was found to be about 10% of total F_m at 760 nm, all the data were corrected. Even after the correction, the spillover ratio in $F\mathrm{I}_{m}$ in State 1 ranged from 21 to 32%, and the spillover ratios were comparable irrespective of growth light conditions. Although extensive grana in low light grown plants would suggest that PSII and PSI are too separated for spillover, in *A. odora* chloroplasts, the ratio of non-appressed thylakoid membranes/total thylakoid membranes was little affected by growth light and more than 40%. Abundant non-appressed thylakoids would contribute to efficient spillover.

Keywords: fluorescence induction, grana, state transitions, sun/shade chloroplasts

Introduction

Land plants are exposed to various light fluctuations. Sudden changes in the photon flux density (PFD) from low to high levels often cause photoinhibition in PSII and PSI (for a recent review, see Kono et al. 2024).

Plants have evolved several mechanisms to protect photosystems from photoinhibition. Leaf and chloroplast movements are effective (Kasahara et al. 2002, Pastenes et al. 2005), yet these are beyond the present scope. The non-photochemical quenching (NPQ), by which chlorophyll excitations are dissipated as heat, has been studied most intensively. Hereafter, chlorophyll and chlorophyll excitation are abbreviated Chl as E*. Changes in the protein structure and the energy levels of the pigments in the PSII antenna systems due to protonation of PsbS protein and conversion of violaxanthin to zeaxanthin, via antheraxanthin, are responsible for NPQ (Bassi and Dall'Osto 2021). It has been proposed that, during NPQ induction, some light harvesting Chl protein complexes (LHCIIs) are clustered and functionally separated from the PSII core complexes, and that E*s in such antenna clusters decay emitting heat (Ruban et al. 2012). It takes 5 to 10 min to induce NPQ mostly at ordinary temperatures. Full conversion of violaxanthin to zeaxanthin takes some more time (Bassi and Dall'Osto 2021). Conversely, when the PFD level is lowered, NPQ is relaxed and the mechanism that dissipates E*s as heat is turned off. The relaxation processes take several minutes as well.

For safe and efficient photosynthesis in the fluctuating light, NPQ should be induced and relaxed rapidly. Kromdijk et al. (2016) overexpressed three components involved in the induction and relaxation processes of NPQ, violaxanthin de-epoxidase, PsbS, and zeaxanthin epoxidase, in *Nicotiana tabacum* (tobacco). When gas exchanges of such leaves were assessed in the laboratory using red and blue LEDs as actinic light, the NPQ relaxation processes were accelerated. In the field, where light fluctuates, these plants grew better than the wild type. Three lines of *Arabidopsis thaliana* overexpressing these three components showed faster NPQ induction and relaxation in the laboratory. However, neither of these lines grew better than the wild type in a natural light greenhouse. In an artificial fluctuating light in a growth chamber, these lines grew less than the wild type (Garcia-Molina and Leister 2020). Although the discrepancy of the results between *N. tabacum* and *A. thaliana* has not been resolved, the strong induction of NPQ might exert a negative effect on photosynthetic production *in A. thaliana* under their experimental conditions (Garcia-Molina and Leister 2020).

We recently found that far-red (FR) light accelerates NPQ relaxation in *A.*

thaliana (Kono et al. 2020). It appears that the H^+/K^+ antiporter in thylakoid membranes (KEA3) is activated by FR light and accelerates NPQ relaxation (Kono et al. unpublished observation). The results of the field experiments by Kromdijk et al. (2016), therefore, would reflect this FR light effect on the rapid NPQ relaxation, because FR light is abundant in natural light.

The state transitions realise balanced distribution of E*s between PSII and PSI by adjusting allocation of mobile LHCIIs between these photosystems. The LHCII movements from PSII to PSI and from PSI to PSII are caused by the phosphorylation and dephosphorylation of LHCIIs and the PSII core, and the responsible kinases have been identified. The state transitions were once thought to play roles in protecting PSII from photoinhibition in high light (Horton and Lee 1985, Anderson and Andersson 1988, Bellafiore et al. 2005). However, it has been revealed that these kinases are inactivated in high light *in vivo* (Rintamäki et al. 1997, Pursiheimo et al. 1998). Moreover, the mutant deficient in one of these kinases, *stn7*, grew well in continuous high light. Since *stn7* did not grow well in the fluctuating light, LHCII phosphorylation may play a role in acclimation to the fluctuating light (Grieco et al. 2012).

The spillover denotes transfer of E*s from PSII to PSI. Analyses of fluorescence induction at 77K revealed that induction of PSI fluorescence occurred synchronously with that of PSII. Spillover occurs even in the absence of closed PSII. When PSII reaction centres close, more E*s are transferred to PSI. This mechanism was first described by Murata (1969). Soon after, theoretical analyses were also made (Kitajima and Butler 1975a, b, Kitajima 1976, Strasser and Butler 1977a, b). Since the spillover prevents accumulation of E*s around the closed PSII reaction centres, the intersystem crossing of the excited Chls in the singlet state (^{S}Chl*s) to those in the triplet state (^{T}Chl*s) around or in the reaction centres is suppressed. Although the energy level of ^{T}Chl* is lower than that of ^{S}Chl*, its lifetime is longer than that of ^{S}Chl* by 3 orders of magnitude (Khorobrykh et al. 2020). Thus, once ^{T}Chl*s are formed, the chance of $^SO_2$ formation increases. Hence, the spillover alleviates PSII photoinhibition. E*s transferred from PSII to PSI oxidize P700 to $P700^+$, the key component for protection of PSI from photoinhibition (Miyake 2020). Therefore, the spillover protects not only PSII but also PSI from photoinhibition (Terashima et al. 2021, Kono et al. 2024).

The extent of NPQ is smaller in shade plant leaves than in sun plant leaves, due to the smaller pool size per leaf area of xanthophyll cycle carotenoids in shade leaves (Demmig-Adams and Adams 2006). Shade plants in the canopy understories are often exposed to sun-flecks (Pearcy 1990) or sun patches (Smith and Berry 2013). To avoid photoinhibition due to such drastic changes in PFD,

spillover would be more efficient than NPQ, because spillover occurs instantaneously while induction of NPQ requires several minutes. Shade plants, therefore, might rely more on the spillover than sun plant leaves to avoid photoinhibition.

After the classical studies for spillover quantification (Kitajima and Butler 1975a, b, Kitajima 1976, Strasser and Butler 1977a, b), there had been few attempts to quantify spillover. Recently, researchers resumed to study spillovers in various organisms using time-resolved fluorescence spectroscopy (Chukhutsina et al. 2019). Megacomplexes have been attracted attention, and the spillover is claimed to occur in the PSI-PSII megacomplexes, which include the PSI, PSII and LHC complexes (Yokono et al. 2015, Ifuku 2023, Kim et al. 2023). If this is true, transfer of E*s would occur in the single membrane because the megacomplex exists in a single thylakoid membrane.

Thylakoid membranes are categorized into appressed and non-appressed membranes. The appressed membranes occur inside the grana in contact with other appressed membranes, while the non-appressed membranes directly face the stroma, forming the inter-grana thylakoids or the grana surface membranes. In the thylakoid membranes, there are some major protein complexes, and their distributions are heterogeneous (Anderson and Andersson 1988). PSII complexes are mainly in the appressed membranes, while PSI complexes and H^+-ATPases are mainly in the non-appressed membranes. Since the PSII complexes in the appressed membranes are located distant from the PSI complexes in the non-appressed membranes, it would be unlikely for E*s to be transferred from PSII to PSI across the membranes. Yet, the transfer of E*s across the membranes was claimed to occur based on measurements of electrogenicity in thylakoid preparations (Trissl et al. 1987).

It is known that the chloroplast morphologies are different between sun and shade plants. Grana in shade plant chloroplasts are generally thicker and contain more thylakoids (Anderson 1986, Björkman 1981). Similar trends have been reported for sun and shade leaves of the same species (Anderson 1986, Björkman 1981), and for the adaxial and abaxial parts in the same leaf (Skene 1974, Terashima et al. 1986). These morphological features imply that spillover would occur more easily in sun-type chloroplasts that have thinner grana. Chow et al. (1988) showed an electron micrograph of gigantic grana in a leaf of low-light grown *Alocasia macrorrhiza*, a shade-tolerant Araceae species. The number of thylakoids per granum exceeded 100. These impressive grana suggest that the spillover of E*s from PSII to PSI might be hampered.

In a recent paper, in which the spillover in *Pinus sylvestris* (Scots pine) leaves was detected by the time-resolved fluorescence analysis, the authors

201 claimed that the increase in the spillover was accompanied by the decrease in the
202 number of thylakoids per granum or by thylakoid de-stacking (Bag et al. 2020).
203 Yokono et al. (2019) surveyed the existence of the megacomplexes in various
204 green plants and found that sun plants accumulate more PSI-PSII megacomplexes
205 than shade plants. They found a tendency that PSI of sun plants had deeper traps
206 (low-energy Chls) to receive excitation energy and showed PSI fluorescence
207 maxima at wavelengths longer than 730 nm. Unfortunately, typical shade-tolerant
208 plants were not included in their plant materials (Table 1 of Yokono et al. 2019).
209 Based on the spectroscopic evidence of the deep-trap Chl *a* in leaves of a shade-
210 tolerant *Alocasia odora*, we proposed that the shade-tolerant plants also have
211 PSI-PSII megacomplexes and, due to the deep-trap Chl *a*, spillover of the
212 excitation energy from PSII to PSI would contribute to formation of $P700^+$ in
213 high light (Terashima et al. 2021, Kono et al. 2024).
214 In the present study, we grew sun species such as *Spinacia oleracea* (spinach)
215 and *Cucumis sativus* (cucumber), and a shade-tolerant species, *Alocasia odora* at
216 different light levels. *Hordeum vulgare* (barley), a wild type and a Chl *b*-less
217 mutant lacking most LHCIIs, were also grown. We measured the induction of PSII
218 fluorescence at 690 nm and that of mostly PSI fluorescence at 760 nm in leaf
219 discs of these plants frozen at 77 K. We divided PSI fluorescence into the
220 fraction corresponding to the PSI fluorescence caused by E*s spilt over from PSII
221 and the intrinsic PSI fluorescence. The spillover ratios were compared among the
222 species and between the growth light levels. A substantial spillover was detected
223 in the leaves of low light grown *A. odora*. Moreover, the spillover was not
224 necessarily greater in high light grown plants. The barley *b*-less mutant also
225 showed considerable spillover. Effects of NPQ induction and $P700^+$ formation on
226 the intrinsic PSI fluorescence were also investigated using low light grown *A.*
227 *odora*. Since the differences in ultrastructure of between the chloroplasts from
228 high and low light grown *A. macrorrhiza* (Chow et al. 1988) were intriguing, we
229 quantitatively analyzed the thylakoid ultrastructure of *A. odora* to elucidate the
230 interrelationship between the ratio of non-appressed thylakoid membranes to total
231 thylakoid membranes, thylakoid stacking, and the spillover. During the present
232 study, we found substantial leftover PSII fluorescence at 760 nm. We tried to
233 quantify the leftover PSII fluorescence and its effect on the estimation of the
234 spillover. The effect of excitation of PSI fluorescence by PSII fluorescence was
235 also considered.

236

Results

Fluorescence induction

The leaf disc on wet paper was illuminated with LEDs peaked at 720 nm (PSI light) or 470 nm (PSII light) at a photon flux density of 10 or 5 μmol m^{-2} s^{-1} for at least 30 min to allow transitions to State 1 or State 2. The disc was then placed in an aluminum cup, kept in the dark for 1.5 to 2 min, and frozen to 77 K. Induction of fluorescence excited by blue light at 460 nm at 50 μmol m^{-2} s^{-1} was measured either at 690 nm or 760 nm for PSII fluorescence ($F690$) or mostly PSI fluorescence ($F760$) at 1 ms time intervals for 30 s. $F690$ and $F760$ both showed typical inductions (Fig. 1A). It took about 5 s to attain F_m levels. When $F760(t)$ was plotted against $F690(t)$, a linear line was obtained (Fig. 1B). See Table 1, for the plant materials. For the measurement system, see Figs. S1 and S2.

For simplicity, let us first assume that fluorescence signals detected at 690 nm and 760 nm were exclusively from PSII and PSI, and that the induction of $F760$ is attributed to the spillover of E*s from PSII (Kitajima and Butler 1985, Butler and Kitajima 1985, Kitajima 1986, Strasser and Butler 1987a, b). $F760(t)$ is, then, expressed as:

$$F760(t) = F760_{\alpha} + \sigma F690(t) \qquad \text{Eq. 1.}$$

where σ is the spillover coefficient, which is equal to the ratio of variable fluorescence at 760 nm to that at 690 nm, $F760_v/F690_v$. When F_m was attained:

$$\begin{aligned} F760_m &= F760_{\alpha} + \sigma F690_m \\ &= F760_{\alpha} + F760_{\beta} \end{aligned} \qquad \text{Eq. 2.}$$

Then the proportion of the spillover in PSI fluorescence was calculated as $F760_{\beta}$ / $F760_m$ or $F760_{\beta}$ / ($F760_{\alpha}$ + $F760_{\beta}$). For a diagrammatical explanation of the relationships between $F760$ and $F690$, see Fig. S3.

The effects of growth light and State transitions on $F690_v/F690_m$ and $F760_v/F760_m$ are shown in Table 1. Except for one case of the HL grown *A. odora*, the differences in $F690_v/F690_m$ depending on the States were not statistically significant, while $F760_v/F760_m$ was greater in State 1. The effects on $F690_m$, $F760_{\alpha}$, and $F760_m$ are shown in Table S1. In these calculations, we assumed that there was no leftover PSII fluorescence (FII) at 760 nm. When the data for the same leaf materials were compared, $F690_m$ was always greater in State 1,

consistent with the view of LHCII movement from PSI to PSII in State 1 light. Inversely, PSI intrinsic fluorescence level ($F760_{\alpha}$), intrinsic PSI fluorescence, was greater in State 2. $F760_m$ is the sum of $F760_{\alpha}$ and that is caused by the spillover from PSII, $F760_{\beta}$. $F760_{\alpha}$ was greater in State 2, while $F760_{\beta}$ would be greater in State 1, which resulted in the situation where there was no consistent effect of the State on $F760_m$. These trends are relevant even when the leftover *F*II at 760 nm was considered (see Table 3, Fig. 4 and Table S2).

We also examined the induction time course (Table S1). Mobile LHCIIs would move from PSII to PSI in State 2 light and *vice versa* in State 1 light. Then, faster induction of *F*690 was expected to occur in the State 1, because antenna size per PSII reaction centre would increase in State 1. When HL and LL leaves were compared, Chl *a*/*b* was lower in LL leaves (Table 1), indicating that LHCIIs were more abundant in LL leaves. Thus, the induction would be faster in LL leaves. Both of these trends were seen (Table S1).

Effects of the leftover PSII fluorescence (*F*II) at 760 nm

Hereafter, we use *F*I and *F*II to denote PSI and PSII fluorescence. Fluorescence emission spectra of the PSI particles at 77K (Lamb et al. 2018 and the references therein) indicate that there may be no PSI fluorescence (*F*I) at 690 nm. On the other hand, the PSII particles show some *F*II at 760 nm. When the PSI complexes having low energy level sinks are present together, however, E*s in the PSII complexes would be more preferentially transferred to such sinks. Thus, in the samples of high integrity, such as gently prepared thylakoids or leaf discs, E*s in PSII could be more efficiently transferred to PSI.

To assess the leftover *F*II at longer wavelengths beyond the *F*I peak, we measured fluorescence at wavelengths ranging from 690 to 780 nm. If there is *F*II at long wavelengths, F_v/F_m will increase with the decrease in PSI fluorescence, because FII_v/FII_m is greater than FI_v/FI_m. We also measured fluorescence emission spectra of F_m in the leaf discs with a photodiode-array spectrophotometer. In these measurements, the leaves of *C. sativus*, *S. oleracea* and *A. odora* were used. The leaf discs were frozen after illumination of the State 1 light, because *F*II and thereby possible leftover *F*II would be enhanced in State 1.

Fig. 2A shows emission spectra of F_m in the State 1. *C. sativus* and *A. odora* showed peaks at 740 nm, while the peak of *S. oleracea* occurred at 737 nm. The spectra for F_v/F_m in the State 1 are shown in Fig. 2B. At 690 nm, F_v/F_m in *S. oleracea* was low, indicating some chronic photoinhibition. These materials were different

313 from those shown in Table 1 (see Materials and Methods). In all these samples,
314 F_v/F_m decreased towards 750 nm and then F_v/F_m increased, indicating presence of
315 leftover *F*II.
316 Since we used leaf discs, reabsorption of fluorescence by Chl distorted the
317 spectral shape at short wavelengths. However, the fluorescence data at the long
318 wavelengths can be used for quantitative analyses. Because many PSII fluorescence
319 data of isolated LHCII and the PSII particles, except for those with obvious
320 contamination of PSI components, show monotonous decreases towards the long
321 wavelengths (Lamb et al. 2018 and the references therein), we assumed that the
322 leftover FII_m can be expressed as a linear function of λ for a narrow range (750 nm
323 $\leq\lambda \leq$ 780 nm). Then, $FI_m(\lambda)$ was expressed as $F_m(\lambda)-FII_m(\lambda)$. F_v/F_m at λ was also
324 expressed with $F_m(\lambda)$, $FII_m(\lambda)$, FII_v/FII_m and FI_v/FI_m (for details, see the
325 supplementary text 1). Assuming FII_v/FII_m was equal to F_v/F_m at 690 nm, we obtained
326 a set of three independent variables, the slope and the intercept of the linear function
327 expressing $FII_m(\lambda)$, and FI_v/FI_m, which minimized the residual sum of squares of the
328 differences (RSS) between the modelled and measured F_v/F_m values at 750, 760, 770
329 and 780 nm. The FI_v/FI_m values and the ratios of FII_m to total F_m at 760 nm, thus
330 obtained, are shown in Table 2. We used all the measured F_v/F_m values for the
331 calculations. Probably because of scattering of the data, the FI_v/FI_m value obtained
332 for *C. sativus* was not statistically significant. When the mean F_v/F_m values for four
333 wavelengths were used, however, a statistically significant value was obtained. For
334 *A. odora* and *S. oleracea*, all the data were used. At 760 nm, FII_m was estimated to
335 be 6% of F_m for *A. odora* and 11% for *S. oleracea* and *C. sativus*. For the fitting of
336 the data, see Fig. S4. Although changes of F_v/F_m with wavelength were not simple,
337 the modelled values followed the measured values well.
338 Spillover ratios are shown in Fig. 3 and Table 3. The data in Fig. 3 were
339 calculated assuming no *F*II leftover at 760 nm. For the spillover ratios assuming
340 0, 5, 10, and 20% FII_m/F_m at 760 nm, see Table 3. As expected from $F760_v/F760_m$
341 data in Table 1, spillover ratios were consistently greater in State 1 light. When
342 HL and LL discs were compared, the levels were comparable in *S. oleracea*. But
343 in *C. sativus* and *A. odora*, the values were significantly greater in LL discs. The
344 leaves of shade tolerant *A. odora* showed the value of more than 0.3 in State 1.
345 The *b*-less barley mutant also showed considerable spillover above 0.3. It is
346 noteworthy that there were no effects of the State light on fluorescence data in
347 the *b*-less barley, in which LHCIIs are mostly absent.
348 Effects of *F*II leftover at 760 nm on the spillover ratios in PSI fluorescence
349 are shown in Table 3. For a given leftover ratio, if we assume FII_v/FII_m is
350 identical to $F690_v/F690_m$, FI_v/FI_m and the spillover ratio (FI_β/FI_m) can be

351 calculated. When the leftover was 10%, spillover ratios in State 1 ranged from 21
352 to 32%. We did not examine leftovers of *F*II in either of the wild type or in the
353 Chl *b* less mutant, the data of these materials in Fig. 3 and Table 3 should be
354 viewed, keeping this in mind.
355
356 **Effects of NPQ**
357
358 Effects of NPQ formation on spillover were examined in the leaf discs from LL *A.*
359 *odora* leaf discs (Fig. 4 and Table S2). After the induction of NPQ by a white
360 light at 700 μmol m^{-2} s^{-1} for 270 s at a room temperature of ca. 23℃, NPQ
361 values, $(FII_m - FII_m')/ FII_m'$, were measured. Then, weak PSI light (at 720 nm)
362 was given for 10 s to oxidise the acceptor side of PSII, and the leaf disc was
363 frozen.
364 Compared with sun plants, NPQ is modest in shade tolerant plants mainly due
365 to the lower contents of xanthophyll cycle carotenoids per leaf area (Demmig-
366 Adams and Adams III 2006). Although LL *A. odora* was used and the actinic light
367 was moderate, NPQ levels after the NPQ induction more than 1.2 were obtained.
368 The differences in NPQ between the samples for $F760_v/F760_m$ (1.22 ± 0.119, n =
369 4) and for $F690_v/F690_m$ measurements (1.35 ± 0.090, n = 4) were not statistically
370 significant (P = 0.194, *t*-test). The data in Fig. 4, which were calculated
371 assuming 0% FII_m leftover at 760 nm, show smaller FI_β and FI_β /FI_m in the NPQ-
372 induced leaf discs, indicate that the spillover of E*s from PSII to PSI decreased
373 after the NPQ induction. FI_β /FI_m in the dark treated control was 0.3, which
374 resembled the value in State 2 light in LL *A. odora* (Fig. 3), as Weis (1985)
375 pointed out for *S. oleracea*. It is also noteworthy that FI_α was unaffected by
376 NPQ. The effects of *F*II leftover at 760 nm on these data are shown in Table S2.
377 The absolute value of the spillover ratio decreased with the increase in the
378 leftover *F*II. It is noteworthy that FI_α was calculated to be constant irrespective
379 of the leftover ratios and NPQ induction by the equations used (see the notes for
380 Table 3).
381
382 **Effects of $P700^+$ on PSI intrinsic fluorescence**
383
384 To detect PSI intrinsic fluorescence, we used a pulse-modulated
385 measuring/actinic beam that was peaked at 700 nm and at the PFD level of 0.07
386 μmol m^{-2} s^{-1}. Changes in the intrinsic PSI fluorescence are shown in Fig. 5. After
387 15 s from the onset of recording at 4 ms intervals, the measuring/actinic light
388 was on. First, no noise reduction circuit was used to examine whether there was

389 an induction in the PSI intrinsic fluorescence. Even though the measuring/actinic
390 light was very weak, no induction was observed in both *A. odora* and *S. oleraea*
391 (Fig. 5A and B). When an unmodulated blue light at 58 μmol m^{-2} s^{-1} was added,
392 the fluorescence level increased to a small extent. This increase was not
393 synchronized with the increase in $P700^+$ (Fig. 5C and D). Moreover, the
394 fluorescence levels did not respond to further increases in the PPFD level.
395 Therefore, the increase in the 'PSI' fluorescence on the addition of the blue light
396 would not be related to $P700^+$. Instead, a slight increase in the 'PSI' fluorescence
397 upon the blue light illumination might reflect the PSII fluorescence induction and
398 fluorescence caused by spillover E*s from PSII to PSI. It is probable that the
399 light used for PSI excitation slightly excited PSII. PSII reduction proceeded
400 slowly, because the measuring/actinic beam had a narrow peak at 700 nm and was
401 weak. Judging from the induction shown in Fig.1, PSII would be fully reduced
402 within 5 s upon illumination of the blue light at 58 μmol m^{-2} s^{-1}. Thus, the PSII
403 fluorescence level excited by the modulated measuring/actinic light would
404 increase. PSI fluorescence caused by the spillover from PSII contributed to this
405 small increase. Once PSII reaction centres were all reduced, further increases in
406 the 'PSI' fluorescence attributable to closure of PSII were not observed even in
407 the stronger actinic lights.
408 $P700^+$ increased slowly in the weak measuring/actinic light and more rapidly
409 with 58 and 360 μmol m^{-2} s^{-1} blue light (Fig. 5C and D). A further increase in the
410 actinic light to 3000 μmol m^{-2} s^{-1} did not cause a notable increase in $P700^+$,
411 indicating that the $P700^+$ level was nearly saturated. When the 'PSI' traces are
412 compared with those for the $P700^+$, there were no indications of fluorescence
413 changes with the increase in $P700^+$. Upon illumination with 3000 μmol m^{-2} s^{-1}
414 light, some decreases in 'PSI' fluorescence were observed both in spinach and *A.*
415 *odora*.
416
417 **Effects of PSII fluorescence on PSI fluorescence**
418
419 Because the *F*II emission spectrum overlaps with the absorption band of Chl *a*,
420 some *F*II is absorbed by long waveband Chl *a* molecules in PSI. Then, *F*I would
421 be caused not only by the spillover E*s from PSII to PSI but also directly by
422 *F*II . In this section, the leftover of *F*II at 760 nm will not be considered for
423 simplicity.
424 In our measuring system, the measuring/actinic light was illuminated from one
425 side of the leaf disc and fluorescence emitted from the same side was measured
426 (Fig. S1). Chls were excited with the pulse-modulated blue light at 460 nm and
427 *F*II and *F*I were measured at 690 and 760 nm. Using a simple model, we

428 calculated 460 nm light absorbed by a thin layer, emission of PSII fluorescence
429 by this layer, re-abosorption of this fluorescence by the rest of the leaf, and
430 emission of PSI fluorescence due to the reabsorption, in this order. Then, the
431 ratio of the *F*I excited by *F*II to the *F*I directly driven by the 460nm light was
432 calculated (see the supplementary text 2 and Fig. S5). The calculations indicate
433 that this ratio should increase with the Chl concentration per leaf area or the Chl
434 concentration in the thylakoid suspension (Fig. S7). If excitation of PSI by *F*II is
435 substantial, then the 'apparent' FI_v/FI_m should increase with the Chl
436 concentration because FII_v/FII_m is greater than FI_v/FI_m. We examined this
437 possibility by plotting $F760_v/F760_m$ of the suspensions of spinach thylakoids of
438 varying Chl concentrations in a 3 mm thick aluminum cup (see Fig. 6A and Fig.
439 S1). We also plotted the $F760_v/F760_m$ against the Chl content in the leaf discs
440 used for Fig. 3 (See Table 1 for Chl contents and Chl *a*/*b* ratios of the samples).
441 We found no dependences of $F760_v/F760_m$ on the chlorophyll content in the
442 sample (Fig. 6A and B). These results indicate that the effect of PSI excitation by
443 *F*II was small in the present measurement. This would be attributed to low PSII
444 fluorescence yield *in vivo*, which is a few percent (Latimer et al. 1957, Lamb et
445 al. 2018).
446
447 **Chloroplast ultrastructure of *A. odora***
448
449 In Fig. 7, electron micrographs of the chloroplasts in the leaves from the *A.*
450 *odora* plants grown at 180 (HL) and 10 (LL) μmol m^{-2} s^{-1} are shown. These
451 chloroplasts were from the first cell layers in the palisade tissues to avoid the
452 effects of intra-leaf light gradient on thylakoid morphologies (Skene 1974,
453 Terashima et al. 1986, Terashima and Hikosaka 1995). Thylakoid membranes per
454 unit volume were more abundant in LL chloroplasts than in HL chloroplasts. Near
455 the chloroplasts, peroxisomes (P) and mitochondria (M) were observed in both
456 samples (Fig. 7 A and B). Starch grains (S) and lipid components (plastoglobules)
457 were more conspicuous in HL chloroplasts (Fig. 7A) than in LL chloroplasts (Fig.
458 7B). In both samples, directions of the grana stacks were variable. Thus, both
459 circular face views and side views of grana stacks were seen within the same
460 sections. The diameters of grana were greater in the LL chloroplasts than in HL
461 chloroplasts. The number of thylakoids per granum was somewhat smaller in LL
462 chloroplasts than in HL chloroplasts. In HL chloroplasts, huge grana with
463 numerous thylakoids were occasionally observed. In these huge grana, some
464 thylakoids were swollen, and, in places, stackings were not tight. In both
465 chloroplasts, there were abundant inter-grana thylakoids.
466 In Fig. 8A. the total length of thylakoid membranes per 1 μm^2 of the ultrathin

467 sections are shown. As already described above (Fig. 7), thylakoid membranes
468 were more packed in the LL chloroplasts than in HL chloroplasts. The
469 quantitative analysis of the ratios of non-appressed membrane/total thylakoid
470 membranes (Fig. 8B) revealed that the ratios were similar between HL and LL
471 chloroplasts: The inter-grana thylakoids were abundant in both HL and LL leaves.
472 For the method used for the measurement of the lengths of non-appressed and
473 appressed membranes, see Figs. S9 and S10.
474

475 **Discussion**

476

477 **Quantitative analyses of the spillover**

478

479 Recent studies on the spillover have been employing the time-resolved
480 fluorescence spectral analysis (Yokono 2015, Bag et al. 2020). Although time
481 scales of spillover and the roles of respective pigments have been clarified by
482 this method, quantitative analyses of the quantum yield of the spillover may not
483 be feasible. For example, it is hard to estimate how much of E*s move from PSII
484 to PSI, although an attempt to measure the quantum yield of spillover in mixtures
485 of cyanobacterial PSI and PSII preparations based on the steady-state and time-
486 resolved fluorescence spectroscopy has been recently reported (Akhtar et al.
487 2024). Classically, slower changes of fluorescence at 77K were analyzed
488 (Kitajima and Butler 1975a, b, Kitajima 1976, Strasser and Butler 1977a, b). We
489 followed these classics. We also dealt with the *F*II leftover beyond the *F*I peak,
490 which was neglected in these classical studies.

491 As shown in Fig.1, in the time scale of the present study, inductions of PSI
492 and PSII fluorescence were synchronous as has been shown (Kitajima and Bulter
493 1975b). Thus, we attributed the main part of PSI induction to the spillover of
494 excitations from PSII. We also assumed that spillover occurs in the absence of
495 closed PSII (Kitajima and Bulter 1975 a, b, Strasser and Butler 1977b). For the
496 diagram of these relationships between *F*I and *F*II, see Fig. S3. We assumed that
497 FI_{α} is constant, which would be supported by the data shown in Figs. 4 and 5.
498 The mathematical equations used for the calculation of FI_{α} give constant FI_{α} at
499 any leftover ratios. The constant FI_{α} values shown in Figs. 4 and 5, thus,
500 inversely support the relevance of our simple equations shown in the note for
501 Table 3.

502 Although these classical studies neglected the F*II* leftover at the long
503 wavelengths, we found the substantial leftover of *F*II at 760 nm. Unfortunately,
504 we could not devise a direct method to quantify the F_v/F_m leftovers. However, we
505 tried to quantify the leftovers from F_m and F_v/F_m spectra, based on the simple
506 assumptions (see the supplementary text 1). Our estimations of the PSII leftovers
507 were 6% for *A. odora*, and 11% for *S. oleracea* and *C. sativus*. Probably these
508 values should not be regarded as values specific to the species. Instead, these
509 may be regarded as examples.

510 The contribution of spillover to *F*I is summarized in Fig. 3. The lowest value
511 was recorded for the HL grown *A. odora* treated in State 2 light. However, this
512 was still more than 0.24. The highest values approached 0.38 in State 1 light.
513 After the correction for the 10% FII_m/F_m at 760 nm, these values were 0.17 and

514 0.32, respectively (Table 3).

515 One of the main aims of the present study was to examine whether the
516 spillover occurs in LL acclimated chloroplasts. Considerable spillover occurred
517 in the shade tolerant plant *A. odora*, and the spillover ratio in this plant was
518 greater in the LL-leaf than in the HL-leaf. In *C. sativus* as well, the LL leaf
519 showed higher spillover ratios, while *S. oleracea* the spillover values were
520 similar.

521 When NPQ was developed, the spillover from PSII to PSI became smaller. It is
522 also noteworthy that FI_{α} was unaffected, indicating that NPQ did not develop in
523 the PSI antennae or its effect was negligibly small in PSI. In *Chlamydomonas*
524 *reinhardii*, the protonated LHCSR3 is involved in energy dissipation in both PSI
525 and PSII antennae (Tokutsu et al.2013, Girolomonia et al. 2019). However, its
526 close homologs are not found in land plants.

527 Using the time-resolved fluorescence spectral analysis, it has been shown that
528 the excited state of deep-trapped Chl *a* is quenched by $P700^+$ in the PSI-PSII
529 megacomplex prepared from *Arabidopsis thaliana* (Yokono et al. 2019). It is
530 inferred that PSI fluorescence is quenched in the presence of $P700^+$. For the
531 Förster resonance transition of the excitation from the excited pigment A to B to
532 occur, the fluorescence emission spectrum of A should overlap with the
533 absorption spectrum of B. The probability is also proportional to the inverse of
534 the sixth power of the distance between these pigments (Blankenship 2021).
535 Because $P700^+$ has a broad absorption band (Inoue et al. 1973), which well
536 overlaps with the PSI fluorescence emission spectrum from red Chls, Förster
537 resonance transition would be possible from E*s to $P700^+$. When this transition
538 occurs efficiently, quenching of PSI fluorescence with the increase in $P700^+$ may
539 be expected. However, appreciable quenching was not detected in LL-grown *A.*
540 *odora* or *S. oleracea* (Fig. 5), probably because the quenching was subtle if any,
541 due the longer distance from the red Chls to P700 (more than 6 nm) than the
542 distance (~ 4.2 nm) in cyanobacteria (Karapetyan et al. 1999, Schlodder et al.
543 2005).

544 On the other hand, in the P700-enriched particles (Ikegami 1976) and the PSI
545 preparation (Wientjes and Croce 2012), $P700^+$ increases the PSI fluorescence
546 level. Although Ikegami (1976) found a considerable increase in PSI fluorescence
547 in his PSI particle, having the Chl/P700 ratio of 7, he argued that this much
548 increase would be hidden in the thylakoids. Wientjes and Groce (2012) detected a
549 4% increase in PSI fluorescence with the formation of $P700^+$ in their PSI
550 preparation in which the chlorophyll/P700 ratio would be around 130. In the data
551 shown in Fig. 5, we were not able to detect the effects of P700 oxidation level on
552 PSI intrinsic fluorescence level. Thus, at least for the first approximation, we

would be able to regard FI_{α} as a constant.

PSI would be excited by PSII fluorescence. The ratio of the PSI fluorescence excited by PSII fluorescence ($FI_{\leftarrow F_{II}}$) to the PSI fluorescence directly excited by the 460 nm light (FI_{direct}) increases with the Chl content per unit area (See the supplementary text 2 and Fig. S7). Then, FI_v/FI_m should also increase with the increase in the Chl content per area. However, this trend was not observed (Fig. 6). $FI_{\leftarrow F_{II}}/FI_{direct}$ may be expressed by Eq. S14 (see the supplementary text 2), which is the product of the yield of PSII fluorescence and the ratio of the integrals. The former would be a few percent (Latimer et al. 1956, Lamb et al. 2018). The latter would be less than 1~2. Thus, $F_{I\leftarrow F_{II}}/F_{I\,direct}$ would be negligible.

Concerning the procedures of the present study, it had been better to measure the 'mostly' PSI fluorescence at 750 nm instead of 760 nm. Then, the overestimations of spillover ratios were smaller. The F_v/F_m spectra had to be measured first, and then the wavelength for the mostly PSI fluorescence measurement had to be determined. The system used in the present study is not ideal for such measurements. The time-resolved fluorometer that can measure the time-dependent spectral transient from F_0 to F_m such as used in Franck et al. (2002) or Santabarbara et al. (2019) should be used. Then, the full spectra can be measured with one leaf disc. Based on the present study, we propose the important procedures needed for accurate quantification of the spillover.

Spillover in fluorescence quenching analyses

Fluorescence is a useful probe to analyse photosynthetic reactions (Papageorgiou and Govindjee 2004). However, in many fluorescence models, spillover is not considered. Let us assume that the initial allocation of E*s to PSII is Ψ_{II}. Maximum quantum yield of PSII photochemistry on absorbed PFD (Φ_{II}), with no energy dependent quenching (NPQ), may be expressed as follows (Kono et al. 2024). In the present consideration, we deal with FII_0 and FII_m only.

$$\Phi_{II} = \Psi_{II} \cdot \frac{k_P}{k_P + k_F + k_D + k_{isc} + k_S} = \Psi_{II} \cdot \frac{k_P}{\sum k} \qquad \text{Eq. 3}$$

where k's are the first-order rate constants: k_P, photochemistry; k_F, radiative (fluorescence) deexcitation; k_D, thermal deexcitation to the ground state via pathways other than NPQ (non-photochemical quenching); k_{isc}, intersystem crossing leading to formation of ^{T}Chl*; and k_S spillover to PSI. Let us assume

that the quantum yield of $F\mathrm{II}_v/F\mathrm{II}_m$ with fully oxidised PSI in low light is 0.8:

$$F\mathrm{II}_v/F\mathrm{II}_m = k_P/\sum k = 0.8 \qquad \text{Eq. 4}$$

Thus,

$$(k_F + k_D + k_{isc} + k_S)/\sum k = 1 - k_P/\sum k = 0.2\,. \qquad \text{Eq. 5}$$

In weak light, PSI quantum yield on absorbed PFD basis, Φ_{I}, is expressed as follows:

$$\Phi_{\mathrm{I}} = 1 - \Psi_{\mathrm{II}} + (k_S/\sum k)\cdot\Psi_{\mathrm{II}} \qquad \text{Eq. 6}$$

We may assume that Φ_{II} and Φ_{I} are identical in weak light for the smooth linear electron transport to occur. Then,

$$\Phi_{\mathrm{I}} = 0.8\cdot\Psi_{\mathrm{II}}. \qquad \text{Eq. 7}$$

As the spillover ratios in State 1 with closed PSII, after the correction for 10% $F\mathrm{II}_m/F_m$ at 760 nm, ranged from 0.210 ~ 0.315 (Table 3):

$$\frac{F\mathrm{I}_\beta}{F\mathrm{I}_a + F\mathrm{I}_\beta} = \frac{\frac{k_S}{k_F+k_D+k_{isc}+k_S}\cdot\Psi_{\mathrm{II}}}{\left(1-\Psi_{\mathrm{II}}+\frac{k_S}{k_F+k_D+k_{isc}+k_S}\cdot\Psi_{\mathrm{II}}\right)} = 0.210 \sim 0.315. \qquad \text{Eq. 8}$$

Noting $\sum k = 5\cdot(k_F + k_D + k_{isc} + k_S)$, we can solve Eq. 7 and Eq. 8. Then, Ψ_{II} ranges from 0.568 to 0.577 and $k_S/\sum k$ ranges from 0.040 to 0.067. In other words, even when PSII reaction centres are all open, 4 to 7% E*s initially allocated to PSII are redirected to PSI. When all the PSII reaction centres are closed, 20 to 27% of E*s initially allocated to PSII are transferred to PSI. Although the relative contribution of spillover decreases with the increase in NPQ, the present analyses confirmed that the spillover ratio is large, and it should not be neglected. It is worth pointing out that considering the lower quantum yield of PSII and spillover, the initial allocation of E*s to PSII should be much greater than 0.5, which is usually assumed in many models.

Chloroplast ultrastructure

Figs. 7 shows chloroplast structure of *A. odora* leaves. As expected, thylakoid

membrane length per unit volume was greater in the chloroplasts in the LL leaf than those in the HL leaf. By dividing these lengths by 2, the thylakoid lengths are obtained. Although some swelling was observed in HL thylakoids, assuming a thylakoid thickness of 13 nm (Kirchhoff 2019), the thylakoid volume per unit chloroplast volume, excluding inter-thylakoid spaces, was calculated as 17% or 25% in HL or LL chloroplasts.

For the Förster-type transfer to occur, the set of pigments should be located close enough. For Chls, the distance which allows 50% probability of energy transfer is calculated to be 5~10 nm (Van Grondelle et al. 1994), then the jump across the inter-thylakoid partition (~ 4 nm, according to Kirchihoff 2019) would be possible. Then, energy transfer may not be confined to within the same membrane. However, based on analyses of the decay time of fluorescence, it has been argued that the main pathway of the spillover is within the same membrane (Farooq et al. 2016). It is noteworthy that inter-grana thylakoids were extensive and that the fractions of the non-appressed thylakoid membranes were similar and more than 40% in both HL and LL chloroplasts of *A. odora*. Although the grana morphology has been attracted attention (Anderson 1986, Terashima and Hikosaka 1995) and rearrangement of grana in response to light has been shown (Anderson and Andersson 1988, Rozak et al. 2002, Kirchhoff 2019), detailed dynamics of the inter-grana thylakoids have not been examined.

The appressed thylakoid membranes may also accommodate megacomplexes in their margins. For example, the size of a PSI-PSII megacomplex of *Oryza sativa* (rice) is approximately 25 nm in its major axis (Kim et al. 2023) and the diameter of the granum ranges 400 to 600 nm (Fig. 6, see also Kirchhoff 2019). Assuming that the grana diameter is R(nm) and the megacomplexes are aligned in the margin of the thylakoid with their PSI portions outwards, the area of the thylakoid accommodating the megacomplexes is calculated to be $[R^2 - (R - 25)^2]/R^2$. Thus, the marginal area corresponding to 23 to 16% of the appressed thylakoid membrane may accommodate the megacomplexes. Since the area of the appressed thylakoids were 60 and 54% of the total areas for HL and LL chloroplasts (Fig. 8), the membrane area that may accommodate the PSI-PSII megacomplexes would be 53% (0.40+0.60 x 0.23) and 55% (0.46 + 0.54 x 0.16) of the total membrane areas in HL and LL chloroplasts.

Conclusions and a brief ecological consideration

The present study showed that spillover occurs in all plant materials including LL grown shade tolerant *A. odora*. The organized spillover would occur within the PSI -PSII megacomplexes in the non-appressed thylakoid membranes and in

664 the marginal areas of appressed-thylakoids. It is noteworthy that these parts
665 would comprise more than 50% of the total thylakoid membranes in both HL and
666 LL grown *A. odora*. In nature, shade tolerant species are usually in the green
667 shade. In such green shade, far-red light is enriched (Kono et al. 2020, 2024).
668 Thus, the thylakoids of these plants are in the State 1, and operate photosynthesis
669 at the highest efficiency without NPQ. Upon sudden exposure of such leaves to
670 high light due to sun patches (Smith and Berry 2013) or sun-flecks (Pearcy and
671 Way 2012), E*s initially allocated to PSII would be spilt over to PSI most
672 efficiently. Since the decreased electron flow and increased excitation flow to
673 PSI contribute to formation of $P700^+$, the safe quencher, the spillover would
674 protect both PSII and PSI from photoinhibition by the spillover.
675

Materials and Methods

Plant Materials

Cucumis sativus L. (cucumber) "Nanshin," *Spinacia oleracea* L. (spinach) "Torai," *Alocasia odora* (G. Lodd.) Spach, and *Hordeum vulgare* L. (barley) "Gunilla, Svalöf AB N83-4001," a wild type, and *H. vulgare* "Dornaria, chlorina-f2^{2800}," a chlorophyll *b*-less mutant, were grown in vermiculite in pots in growth chambers at 25°C. Light period was 12 h. Light was provided by a bank of white fluorescent lamps. Photosynthetic photon flux density (PPFD) levels were adjusted with the number of fluorescent tubes and/or the black shade cloth. *C. sativus*, *S. oleracea*, and *A. odora* were grown at two photosynthetic PPFD (400–700 nm) levels. For cucumber and spinach, the PPFD levels were 400 and 100 µmol m^{-2} s^{-1}, while for *A. odora*, 100 and 10 µmol m^{-2} s^{-1} were used. *H. vulgare* plants were grown at 400 µmol m^{-2} s^{-1}. For electron microscopy, *A. odora* grown at 180 and 10 µmol m^{-2} s^{-1} were used. Plants were given the 1/1000 strength of the Hyponex 6–10–5 solution (Hyponex, Japan) diluted with tap water every two or three days. The relative humidity of the chamber was kept above 50%. The growth light PPFD level of 400 µmol m^{-2} s^{-1} for sun plants or crops would be sufficiently high. At 10 µmol m^{-2} s^{-1}, where *A. odora* showed slow growth, corresponds to PPFD levels on the deep forest floor.

For the assessment of *F*II leftover at 760 nm, we grew *A. odora* and *C. sativus* outdoors in the soil in the pots. The *A. odora* plant used was the clone of the plants used in other measurements. For *C. sativus,* the same variety ('Nanshin') was used. We bought *S. oleracea* from a local market. These measurements were conducted in July 2024, the warmest season.

77K fluorescence from leaf discs

Fluorescence induction at 77K was measured with a PAM 101 fluorometer (Walz, Effeltrich, Germany). The original red LED (650 nm) used for the pulse-modulated measuring light was replaced with a blue LED (OSUB5111AST, OptoSupply, Hong Kong) peaked at 460 nm. In the PAM 101 fluorometer, a photodiode was used to detect fluorescence. The original far-red filter was replaced with a 690 nm or 760 nm bandpass filter (HMX0690 or HMX0760, Asahi-Spectra, Tokyo, Japan) for PSII or mostly PSI fluorescence measurements. Leaf discs (10 mm in diameter) were cut with a leaf punch. 16 leaf discs were used for one series of measurements. For one set of measurements, four leaf discs were used, and fluorescence inductions were measured at 690 and 760 nm,

respectively, in States 1 and 2. These four discs were taken from a narrow uniform part of a leaf. For *C. sativus*, *S. oleracea*, and *A. odora* 16 leaf discs were taken from one leaf, whereas, for *H. vulgare*, four sets were taken from four separate leaves. The leaf discs were placed on wet filter paper with the adaxial sides upward and illuminated with State 2 light at 470 nm from LEDs (L470, Ushio, Tokyo) or State 1 light at 720 nm from LEDs (L720, Ushio, Tokyo) at a photon flux density of 10 µmol m^{-2} s^{-1} at a room temperature of ca. 25°C. For *A. odora* leaves grown at 10 µmol m^{-2} s^{-1}, the PFD level was lowered to 5 µmol m^{-2} s^{-1}. After illumination for at least 30 min with either of the State 1 or State 2 LEDs, the adaxial side of leaf disc was attached to a quartz rod with silicone grease and covered with an aluminum cap and dipped in liquid nitrogen in a Dewer jar. From the cessation of the State light treatment until the freezing, all the procedures were made within 1.5 to 2 min in dim light. After the enclosure in the cup, the sample was further darkened. When the temperature of the sample in the aluminum cap was equilibrated with that of liquid nitrogen, which was detectable by a change of the sound of bubbling, recording was started. After 2 s, the measuring/actinic blue light at 50 µmol m^{-2} s^{-1} (pulse modulated at 100 kHz) was turned on. The fluorescence induction at 690 nm or 760 nm was recorded at 1 ms time intervals for 28 s on a USB data acquisition system (USB-1608FS, Measurement Computing, Norton, MA, USA). For the measurement system see Fig. S1. For transmittance spectra of 690 and 760 nm bandpass filters, see Fig. S2.

The F_v/F_m spectra in the wavelength range from 690 to 780 nm were obtained as described above. Emission spectra of F_m, excited by blue light from an LED peaked at 450 nm, were measured using a photodiode array spectrophotometer (C10083CAH, Hamamatsu Photonics, Japan) and an optical system similar to that used for the F_v/F_m measurement. For details, see Terashima et al. (2021) and Fig. S1. F_v/F_m in the leaf discs were measured as described above using the band pass filters (Asahi-spectra). The leaf discs were treated in State 1 light at 720 nm at 10 µmol m^{-2} s^{-1} at least for 30 min.

Effects of NPQ on the spillover

The effects of NPQ on the spillover were examined using an *A. odora* leaf grown at 10 µmol m^{-2} s^{-1} light. The leaf disc attached to a quartz rod was covered with an aluminum cap, and NPQ was induced by illuminating the leaf disc with an actinic white light from a tungsten lamp (KL1500 lcd, Schott, Mainz, Germany) at 700 µmol m^{-2} s^{-1} for 270 s at a room temperature of ca. 23℃. Saturating flashes at 6,600 µmol m^{-2} s^{-1} for 1 s were given at 20 s intervals. The actinic

754 light was turned off, and 10 s after, the measuring beam was turned off. At 5 s
755 after turning off the actinic light, far-red light peaked at 720 nm at 10 μmol m^{-2}
756 s^{-1} was illuminated for 10 s to oxidise PSII. Then, the leaf disc in the cap was
757 frozen at 77K. When the temperature reached 77K, PSI or PSII fluorescence was
758 measured as above.
759
760 **Effects of $P700^+$ formation on PSI fluorescence**
761
762 PSI fluorescence was obtained by preferential illumination of PSI pigments. The
763 actinic/measuring light was a 700 nm LED (5 mm bullet type, Ushio, Tokyo,
764 Japan) passing through a 700 nm band pass filter with 10 nm half-band width
765 (HMX700, Asahi-spectra, Tokyo, Japan) and a 710 nm short pass filter (SVX
766 710). For detection of PSI fluorescence, the photodiode of the PAM 101 covered
767 with a long pass filter (LVX 730, allowing transmission of far-red light > 730
768 nm) was used. Since it was necessary to use the measuring/actinic light of very
769 narrow waveband, the PFD level at the leaf disc surface was 0.07 μmol m^{-2} s^{-1}.
770 The leaf disc kept in the dark at least for 30 min was attached to the quartz
771 rod, enclosed by an aluminum cup, chilled at 77 K, and its PSI fluorescence was
772 measured. The accumulation of $P700^+$ was measured with a dual-wavelength
773 (820/870 nm) unit (ED-P700DW) attached to a PAM fluorometer (Walz) in the
774 reflectance mode. When the two PAM101 systems were operated at the same time,
775 the signals sometimes became noisy. Thus, we used similar leaf discs taken from
776 the same leaf and measured the PSI fluorescence and redox state of P700
777 separately, but according to the same illumination time schedule.
778 After the onset of recording at 4 ms intervals, the measuring/actinic light for
779 PSI at 0.07 μmol m^{-2} s^{-1} was on at 15 s. The signal damping was started to reduce
780 the noise level at 30 s, an unmodulated blue light at 58 μmol m^{-2} s^{-1} from 460 nm
781 LED was added at 60 s, the blue light level was increased to 360 μmol m^{-2} s^{-1} at
782 80 s, and, the blue light was turned off and a white light from a tungsten lamp at
783 3000 μmol m^{-2} s^{-1} was turned on at 100 s. When the redox state of P700 was
784 measured, the pulse-modulated measuring light from a PAM 101 far-red LED
785 emitting light with wavelengths ranging from 800 to 900 nm was used.
786
787 **Effects of excitation of PSI fluorescence by re-absorbed PSII fluorescence**
788
789 To examine the effects of Chl concentration on PSI fluorescence excited by
790 reabsorbed PSII fluorescence, thylakoids were prepared from the laboratory
791 grown spinach at 400 μmol m^{-2} s^{-1} PPFD (see above) as described in Terashima et
792 al. (2021). PSI fluorescence induction in the thylakoid suspension in a buffer

793 containing 0.3 M sorbitol, 10 mM NaCl, 5 mM $MgCl_2$ and 50 mM and Hepes-KOH
794 (pH at 8.0) was measured at 77K in a 3 mm thick aluminum cuvette (see Fig. S1).
795 All these procedures were made in dim light. The pulse modulated
796 measuring/excitation light at 460 nm used was at the PPFD of 12 μmol m^{-2} s^{-1}.
797 The weaker light was used to obtain more data points for the induction phase
798 with the diluted thylakoid suspensions. For theoretical consideration, see the
799 supplementary text 2.
800
801 **Data processing**
802
803 *F_0 and F_m determination for leaf discs*: The recording system was turned on at 0
804 s, and the measuring/actinic light was turned on at 2 s. The zero (0) and the
805 maximum fluorescence (F_m) levels were obtained by averaging 2000 data points
806 between 0 and 2 s and between 28 s and 30 s. A linear regression equation was
807 obtained using the 50 data points, from 2.005 to 2.054 s. F_0 was obtained by
808 substituting 2 s to this equation.
809 F_m and F_0 thus obtained were used to calculate F_v (= F_m – F_0) and F_v /F_m. As
810 the increases in PSI and PSII fluorescence intensities were synchronous (Fig. 1),
811 the variable fluorescence in PSI was assumed to be attributed to the spillover
812 from PSII variable fluorescence.
813 The spillover from PSII to PSI was assumed to occur at the same efficiency
814 regardless of whether PSII reaction centres were open or closed (Strasser and
815 Butler (1977a, b). Based on these assumptions, and assuming that PSII and PSI
816 fluorescence could be separately measured at 690 and 760 nm, PSI fluorescence
817 at time t, $FI(t)$, was expressed as:
818
819 $$FI(t) = FI_\alpha + \sigma \cdot FII(t). \quad \text{Eq. 9}$$
820
821 Where σ is the spillover coefficient. From this, intrinsic PSI fluorescence (FI_α)
822 was obtained:
823
824 $$FI_\alpha = FI_m - FI_v/(FII_v/FII_m). \quad \text{Eq. 10}$$
825
826 *Induction time determination*: Assuming that the PSII fluorescence induction
827 occurred in two phases, the induction curve was fitted by the equation:
828
829 $$F(t) = F_0 + \cdot a \cdot [1 - exp(-k_1 \cdot t)] + (F_m - F_0 - a) \cdot [1 - exp(-k_2 \cdot t)] \quad \text{Eq. 11}$$
830
831 We used F_0 and F_m, which were obtained as above. A, k_1 and k_2 were obtained by

832 the fitting with KaleidaGraph (Version 5.0, Synergy Software). Then, $t_{1/2}$ was
833 obtained as t giving $F(t) = F_0 + (F_m - F_0)/2$.
834
835 *F_0 determination for thylakoid suspension*: Since a weaker actinic/measuring
836 light was used for thylakoid suspensions, the linear regression of 50 data points
837 was not reliable due to the lower S/N ratio. When the number of data points was
838 simply increased, linearity could not be assumed. Thus, we fitted Eq. 8 to the
839 fluorescence transient for 2 s to obtain F_0, a, k_1 and k_2. Because time constants k_2
840 was always one order of magnitude smaller than k_1, we further assumed that $k_2 =$
841 $0.1 \cdot k_1$. The determination coefficients obtained with this assumption was always
842 greater than that for the equation in which k_1 and k_2 were independently obtained.
843
844 **Electron microscopy**
845
846 The *A. odora* plants used were grown at the PPFD 180 or 10 μmol m^{-2} s^{-1}. After
847 harvesting, the leaves were kept in the dark at a room temperature for at least 30
848 min before fixation. Leaf segments, ca. 1 mm x 4 mm were excised and fixed
849 immediately in 2% glutaraldehyde in 0.05 M potassium phosphate buffer (pH 6.8)
850 and kept at the room temperature for 2 h and then at 4°C overnight. Six rinses in
851 the buffer solution preceded postfixation with 2% OsO_4 in the buffer at room
852 temperature for 2 h. After dehydration in a graded acetone series, leaf materials
853 were embedded in Spurr's resin. The ultrathin sections (silver-gold) were
854 poststained with uranyl acetate and lead citrate and examined with a Hitachi H-
855 7500 transmission electron microscope at an accelerating voltage of 80 kV.
856 Electron-micrographs of the first cell layers of the palisade tissues were taken
857 to avoid the effects of intra-leaf light gradient on thylakoid morphologies (Skene
858 1974, Terashima et al. 1986, Terashima and Hikosaka 1995). In the leaves grown
859 at 180 or 10 μmol m^{-2} s^{-1} light, 36 or 30 chloroplasts were randomly chosen, and
860 in these chloroplasts, 178 or 157 squares of 1 μm^2, in which all thylakoid
861 membranes were in focus, were selected randomly. We randomly selected 10 of
862 these squares from 10 chloroplasts for each growth light level and thylakoid
863 lengths were measured using Fiji/ImageJ (NIH).
864 The total length of the thylakoid membranes per 1 μm^2 was also calculated as
865 an index of thylakoids to stroma volume ratio. The abundance of non-appressed
866 thylakoids was expressed as the ratio of the length of the non-appressed
867 thylakoid membranes to the total thylakoid membranes. For examples of tracing
868 the electronmicrographs, see Figs. S9 and S10.
869
870

Funding

This work was partly supported by grants from Japan Society for the Promotion of Science (17H05718, 19H04718, 22H02640 and 23K23903).

Acknowledgement

The barley seeds were a kind gift of Professor W.S. Chow. We thank Professor W. S. Chow, Dr. D. Y. Fan, Dr. E. Kim, Dr. M. Kitano and Dr. M. Kitajima for constructive comments. We also thank Dr. G. Shansker for drawing our attention to PSI fluorescence excited by PSII fluorescence. We are grateful to Mr. H. Hashimoto and Mr. A. Okamoto, Namoto Co., Ltd., for assisting modification of the PAM 101. We examined the leftover PSII fluorescence at 760 nm in response to the comments by the two reviewers. We thank them for this fundamental comment.

Author Contributions

All authors contributed to this study and are responsible for the content of this paper.

Disclosure

The authors have no conflict of interest.

Supplementary materials

Table S1 *F*II induction time, $F690_m$, $F760_m$, and $F760_a$

Table S2 Effects of the *F*II leftover at 760 nm on fluorescence parameters

Fig. S1. The optical system for the fluorescence measurement.

Fig. S2. Transmission spectra of the 690 and 760 nm band pass filters

Fig. S3. The relationship between F690 and F760 induction assuming no FII leftover at 760 nm.

Text 1: Estimation of the leftover *F*II at 760 nm (with Fig. S4)

Text 2: Is *F*I excited by *F*II? (with Figs. S5, 6, 7 and 8)

Figs. S9 and S10. Electron micrographs of *A. odora* chloroplasts showing how the ratios of non-appressed thylakoid membranes to the total length of thylakoids were measured.

References

Akhtar, P., Balog-Vig, F., Han, W., Li, X., Han, G., Shen, J.-R., Lambrev, P.H. (2024) Quantifying the energy spillover between photosystem II and I in cyanobacterial thylakoid membranes and cells. Plant Cell Physiol. 65: 95-106.

Anderson, J.M. (1986) Photoregulation of the composition, function, and structure of thylakoid membranes. Annu. Rev. Plant Physiol. 37: 93-136.

Anderson, J.M. and Andersson, B. (1988) The dynamic photosynthetic membrane and regulation of solar energy conversion. Trend. Biochem. Sci. 13: 351-355.

Bag, P., Chukhutsina, V., Zhang,Z., Paul, S., Ivanov, A.G., Shutova1, T., Croce, R., Holzwarth, A.R., and Jansson, S (2020) Direct energy transfer from photosystem II tophotosystem I confers winter sustainability in Scots Pine. Nat. Comm. 11: 6388. https://doi.org/10.1038/s41467-020-20137-9

Bassi, R. and Dall'Osto, L. (2021) Dissipation of light energy absorbed in excess: The molecular mechanisms. Annu. Rev. Plant Biol. 72: 47-76.

Bellaflore, S., Barneche, F., Peltler, G. and Rochaix, J.D. (2005) State transitions and light adaptation require chloroplast thylakoid protein kinase STN7. Nature 433: 892-895.

Björkman. O. (1981) Responses to different quantum flux densities. In: Lange, O.K., Nobel, P.S., Osmond, C.B. and Ziegler, H. (eds) Encyclopedia of Plant Physiology, New Series, vol 12A. Springer, Berlin, pp 57–106.

Blankenship, R.E. (2021) Molecular Mechanisms of Photosynthesis. 3rd edn. P. 328. Wiley, Hoboken.

Chow, W.S., Qian, L., Goodchild, D.J. and Anderson, J.M. (1988) Photosynthetic acclimation of *Alocasia macrorrhiza* (L.) G. Don. Aust. J. Plant Physiol. 15:107–122. https:// doi. org/ 10. 1071/ PP988 0107

Chukhutsina, V.U., Holzwarth, A.R., Croce, R. (2019) Time-resolved fluorescence measurements on leaves: principles and recent developments. Photsynth. Res. 140: 3555-369.

Demmig-Adams, B. and Adams III, WW. (2006) Photoprotection in an ecological context: The remarkable complexity of thermal energy dissipation. New Phytol. 172: 11-21.

Farooq, S., Chmeliov, J., Trinkunas, G., Valkunas, L. and van Amerongen, H. (2016) Is there excitation energy transfer between different layers of stacked photosystem-II-con-taining thylakoid membranes? J. Phys. Chem. Lett. 7: 1406–1410. https://
doi.org/10.1021/acs.jpclett.6b00474.

Franck, F., Juneau P., and Popovic, R. (2002) Resolution of the Photosystem I and Photosystem II contributions to chlorophyll fluorescence of intact leaves at room temperature. Biochim Biophys. Acta 1556: 239-246.

Garcia-Molina, A. and Leister, D. 2020 Accelerated relaxation of photoprotection

962 impairs biomass accumulation in *Arabidopsis*. Nat. Plant 6: 9-12.
963
964 Girolomonia, L., Cazzanigaa, S., Pinnola, A., Perozenia, F., Ballottaria, M. and
965 Bassi, R. (2019) LHCSR3 is a nonphotochemical quencher of both photosystems in
966 *Chlamydomonas reinhardtii*. Proc. Natl. Acad. Sci. USA. 116: 4212-4217.
967
968 Grieco, M., Tikkanen, M., Paakkarinen, V., Kangasjärvi, S. and Aro, E.M. (2012)
969 Steady-state phosphorylation of light-harvesting complex II proteins preserves
970 photosystem I under fluctuating white light. Plant Physiol. 160: 1896-1910.
971
972 Horton, P. and Lee, P. (1985) Phosphorylation of chloroplast membrane proteins
973 partially protects against photoinhibition. *Planta* 165: 37-42.
974
975 Ifuku, K. (2023) Diversity of the PSI–PSII megacomplexes that conduct energy
976 spillover in green plants. Plant Cell Physiol. 64: 844-846.
977 doi:https://doi.org/10.1093/pcp/pcad069,
978
979 Ikegami, I. 1976 Fluorescence changes related in the primary photochemical
980 reaction in the P-700-enriched particles isolated from spinach chloroplasts.
981 Biochim. Biophys. Acta 449: 245-258.
982
983 Inoue, Y., Ogawa, T. and Shibata, K. (1973) Light-induced spectral changes of
984 P700 in the 800-nm region in *Anacystis* and spinach lamellae. Biochim. Biophys.
985 Acta 305: 483-487.
986
987 Karapetyan, N.V., Holzwarth, A. and Rögner, M. (1999) The photosystem I trimer
988 of cyanobacteria: molecular organization excitation dynamics and physiological

significance. FEBS Lett. 460: 395-400.

Kasahara, M., Kagawa, T., Oikawa K., Suetsugu, N., Miyao, M. and Wada, M. (2002) Chloroplast avoidance movement reduces photodamage in plants. Nature 420: 829-832.

Khorobrykh, S., Havurinne, V., Mattila, H. and Tyystjärvi, E. (2020) Oxygen and ROS in photosynthesis. Plants 9: 91 doi:10.3390/plants9010091

Kim, E., Yokono, M., Tsugane, T., Ishii, A., Noda, C. and Minagawa, J. (2023) Formation of a stable PSI–PSII megacomplex in rice that conducts energy spillover. Plant Cell Physiol. 64: 858-865. https://doi.org/10.1093/pcp/pcad037

Kirchhoff, H. 2019 Chloroplast ultrastructure in plants. New Phytol. 223: 565-574.

Kitajima, M. (1976) Light-induced redistribution of excitation energy in leaves as observed in terms of fluorescence induction. Plant Cell Physiol. 17: 921-930.

Kitajima, M., Butler, W.L. (1975a) Quenching of chlorophyll fluorescence and primary photochemistry in chloroplasts by dibromothymoquinone. Biochim. Biophys. Acta 376:105–115.

Kitajima, M., Butler, W.L. (1975b) Excitation spectra for photosystem I and photosystem II in chloroplasts and the spectral characteristics of the distribution of quanta between the two photosystems. Biochim. Biophys. Acta 408:297–305.

Kono, M., Kawaguchi, H., Mizusawa, N., Yamori, W., Suzuki, Y. and Terashima, I. (2020) Far-red light accelerates photosynthesis in the low-light phases of

fluctuating light. Plant Cell Physiol. 61: 192–202. https://doi.org/10.1093/pcp/pcz191

Kono, M., Oguchi, R. and Terashima, I. (2024) Photoinhibition of PSI and PSII in nature and in the laboratory: Ecological approaches. Prog. Bot. 84: 241–292. https://doi.org/10.1007/124_2022_67

Kromdijk, J., Głowacka, K., Leonelli, L., Gabilly, S.T., Iwai, M., Niyogi, K.K. and Long, S.P. (2016) Improving photosynthesis and crop productivity by accelerating recovery from photoprotection. Science 354: 857-861. 10.1126/science.aai8878

Lamb, J.J., Røkke, G. and Hohmann-Marriot, M.F. 2018 Chlorophyll fluorescence emission spectroscopy of oxygenic organisms at 77 K. Photosynthetica 56: 105-124.

Latimer, P., Bannister, T.T. and Rabinowitch, E. (1956) Quantum yields of fluorescence of plant pigments. Sicnece 124: 585-586.

Miyake, C. (2020) Molecular mechanisms of oxidation of P700 and suppression of ROS production in photosystem I in response to electron-sink limitations in C3 plants. Antioxidants 9:230. https://doi.org/10.3390/antiox9030.230

Murata, N. (1969) Control of excitation transfer in photosynthesis. I. Light-induced change of chlorophyll a fluorescence in *Porphyridium cruentum*. Biochim. Biophys. Acta 172: 242-251.

Papageorgiou G.C. and Govindjee (2004) Chlorophyll *a* Fluorescence. A Signature of Photosynthesis. p. 818. Springer, Dordrecht.

Pastenes, C., Pimentel, P. and Lillo, J. 2005 Leaf movements and photoinhibition in relation to water stress in field-grown beans. J. Exp. Bot. 56: 425-433.

Pearcy, R.W. (1990) Sunflecks and photosynthesis in plant canopies. Annu. Rev. Plant Physiol. Plant Mol. Biol. 41: 421-453.

Pursiheimo, S., Rintamäki, E., Baena-Gonzalez, E. and Aro, E.M. (1998) Thylakoid protein phosphorylation in evolutionally divergent specieswith oxygenic photosynthesis FEBS Lett. 423: 178-182.

Rintamäki, E., Salonen, M., Suoranta, U.-M., Carlberg, I., Andersson, B. and Aro, E.M. 1997, Phosphorylation of light-harvesting complex II and photosystem II core proteins shows different irradiance-dependent regulation in vivo. J. Biol. Chem. 272: 30476-30482.

Rozak, P.R., Seiser, R.M., Wacholtz, W.F. and Wise, R.R. (2002) Rapid, reversible alterations in spinach thylakoid appression upon changes in light intensity. Plant Cell Environ. 25: 421-429.

Ruban, A.V., Johnson, M.P., Duffy, C.D.P. (2012) The photoprotective molecular switch in the photosystem II antenna. Biochim. Biophys. Acta 1817: 167-181.

Santabarbara, S., Villafiorita Monteleone, F., Remelli, W., Rizzo, R., Menin, B, Casazza A.P. (2019) Comparative excitation-emission dependence of the F_v/F_M ratio in model green algae and cyanobacteria strains. Physiol. Plant. 166: 351-364.

Schlodder, E., Çetin, M., Byrdin, M., Terekhovac, I.V. and Karapetyan, N.V.

(2005) $P700^{+}$- and $^{3}P700$-induced quenching of the fluorescence at 760 nm in trimeric Photosystem I complexes from the cyanobacterium *Arthrospira platensis*. Biochim. Biophys. Acta 1706: 53-67. doi:10.1016/j.bbabio.2004.08.009

Skene, D. S. (1974) Chloroplast structure in mature apple leaves grown under different levels of illumination and their response to changed illumination. Proc. R. Soc. London B 186: 75-78.

Smith, W.K. and Berry Z.C. (2013) Sunflecks? Tree Physiol. 33：233-237.

Strasser, R. and Butler, W.L. (1977a) Energy transfer and the distribution of excitation energy in the photosynthetic apparatus of spinach chloroplasts. Biochim. Biophys. Acta 460: 230-238.

Strasser, R. and Butler, W.L. (1977b) The yield of energy transfer and the spectral distribution of excitation energy in the photochemical apparatus of flashed bean leaves. Biochim. Biophys. Acta 462: 295-306.

Terashima, I., Hikosaka, K. (1995) Comparative ecophysiology of leaf and canopy photosynthesis. Plant Cell Environ. 18: 1111–1128

Terashima, I., Matsuo, M., Suzuki, Y., Yamori, W. and Kono, M. (2021) Photosystem I in low light-grown leaves of *Alocasia odora*, a shade-tolerant plant, is resistant to fluctuating light-induced photoinhibition. Photosynth. Res. 149:69–82.

Terashima, I., Sakaguchi, S. and Hara, N. (1986) Intra-leaf and intercellular

gradients in chloroplast ultrastructure of dorsiventral leaves illuminated from the adaxial or abaxial side during their development. Plant. Cell Physiol. 27: 1023-1031.

Tokutsu, R., and J. Minagawa. (2013). Energy-dissipative supercomplex of photosystem II associated with LHCSR3 in *Chlamydomonas reinhardtii*. Proc. Natl. Acad. Sci. USA 110: 10016-10021

Trrisl, H.-W., Breton, J., Deprez, J. and Leibl, W. (1987) Primary electrogenic reactions of photosystem II as probed by the light-gradient method. Biochim Biophys Acta 893: 305-319.

Van Grondelle, T., Dekker, J.P., Gillbro, T. and Sundstrom V. (1994) Energy transfer and trapping in photosynthesis. Biochim. Biophys. Acta 1187: 1-65.

Weis, E. (1985) Light-and temperature-induced changes in the distribution of excitation energy between Photosystem I and Photosystem II in spinach leaves. Biochim. Biophys. Acta 807: 118-126.

Wientjes, E. and Croce, R. (2012) PMS: Photosystem I electron donor or fluorescence quencher. Photosynth. Res. 111: 185-191.

Yokono, M., Takabayashi, A., Akimoto, S. and Tanaka, A. (2015) A megacomplex composed of both photosystem reaction centers in higher plants. Nat. Comm. 6: 6675. DOI: 10.1038/ncomms7675

Yokono, M., Takabayashi, A., Kishimoto, J., Fujita, T., Iwai, M., Murakami, A.,

1122 Akimoto, S. and Tanaka, A. (2019) The PSI–PSII megacomplex in green plants.
1123 Plant Cell Physiol. 60: 1098-1108.
1124
1125

Table 1. Chl content and Chl *a*/*b* of the samples and the effects of State transitions on $F690_v/F690_m$ and $F760_v/F760_m$

	Growth light μmol m^{-2} s^{-1}	Chl (mmol m^{-2})	Chl *a*/*b*	State	$F690_v$ / $F690_m$	$F760_v$ / $F760_m$
C. sativus	400	0.26 ± 0.024	5.08 ± 0.141 **	1	0.850 ± 0.018	0.319 ± 0.008 ***
				2	0.836 ± 0.019	0.290 ± 0.006
	100	0.25 ± 0.028	4.06 ± 0.080	1	0.824 ± 0.005	0.316 ± 0.009 **
				2	0.823 ± 0.014	0.277 ± 0.014
S. oleracea	400	0.62 ± 0.048 **	3.86 ± 0.073 **	1	0.781 ± 0.033	0.299 ± 0.029 **
				2	0.794 ± 0.019	0.238± 0.012
	100	0.49 ± 0.034	3.59 ± 0.105	1	0.777 ± 0.042	0.297 ± 0.016 **
				2	0.793 ± 0.019	0.244 ± 0.017
A. odora	100	0.63 ± 0.024 **	3.96 ± 0.025 **	1	0.851 ± 0.006 **	0.246 ± 0.018 **
				2	0.810 ± 0.014	0.202 ± 0.009
	10	0.54 ± 0.035	3.52 ± 0.041	1	0.774 ± 0.015	0.265 ± 0.012 **
				2	0.755 ± 0.027	0.224 ± 0.017
H. vulgare WT	400	0.38 ± 0.068 **	3.75 ± 0.194	1	0.822 ± 0.028	0.274 ± 0.025 *
				2	0.797 ± 0.021	0.232 ± 0.009
Chl *b*-less	400	0.18 ± 0.027	>>	1	0.731 ± 0.059	0.238 ± 0.010
				2	0.694 ± 0.017	0.226 ± 0.007

Each of the data is shown as the mean ± S.D. (n = 4). Chl *a*/*b* ratio in the Chl *b*-less barley was not determined and was noted by >>. *, ** and *** denote $P < 0.05$, 0.01, and 0.001, respectively, according to *t*-test.

Table 2. FI_v/FI_m giving the least SSR and the leftover ratio of FII_m/F_m at 760nm

	FI_v/FI_m ± sem				F_v/F_m		FI_v/FI_m	FII_m/F_m
					690 nm	760 nm	$F760_v/F760_m$	at 760 nm
C. sativus	0.155	±	0.098	ns	0.733	0.290	*0.534*	***0.234***
mean values	0.235	±	0.017	*	0.733	0.290	0.810	**0.110**
S. oleracea	0.171	±	0.030	***	0.637	0.222	0.770	**0.109**
A. odora	0.247	±	0.024	***	0.787	0.279	0.885	**0.059**

Table 3 Effects of 0, 5, 10 and 20% FII_m/F_m at 760 nm on FI_v/FI_m and spillover ratio (FI_β/FI_m)

	Growth light (μmol m^{-2} s^{-1})	State	$F690_v/F690_m$	FI_v/FI_m				Spillover ratio			
				0%	5%	10%	20%	0%	5%	10%	20%
C. sativus	400	1	0.850	**0.319**	0.291	**0.260**	0.186	**0.375**	0.306	**0.306**	0.219
		2	0.836	**0.290**	0.261	**0.229**	0.154	**0.347**	0.274	**0.274**	0.184
	100	1	0.824	**0.316**	0.289	**0.260**	0.189	**0.383**	0.315	**0.315**	0.229
		2	0.823	**0.277**	0.248	**0.216**	0.141	**0.339**	0.263	**0.263**	0.171
S. oleracea	400	1	0.781	**0.299**	0.274	**0.245**	0.179	**0.379**	0.314	**0.314**	0.229
		2	0.794	**0.238**	0.209	**0.176**	0.099	**0.287**	0.222	**0.222**	0.125
	100	1	0.777	**0.297**	0.272	**0.244**	0.177	**0.385**	0.314	**0.314**	0.228
		2	0.793	**0.244**	0.215	**0.183**	0.107	**0.308**	0.231	**0.231**	0.135
A. odora	100	1	0.851	**0.246**	0.214	**0.179**	0.095	**0.286**	0.210	**0.210**	0.111
		2	0.810	**0.202**	0.170	**0.134**	0.050	**0.243**	0.166	**0.166**	0.062
	10	1	0.774	**0.265**	0.238	**0.208**	0.138	**0.341**	0.269	**0.269**	0.178
		2	0.755	**0.224**	0.196	**0.165**	0.091	**0.298**	0.219	**0.219**	0.121
H. vulgare	400	1	0.822	**0.274**	0.245	**0.213**	0.137	**0.331**	0.259	**0.259**	0.167
WT		2	0.797	**0.232**	0.202	**0.169**	0.091	**0.294**	0.212	**0.212**	0.114
H. vulgare	400	1	0.731	**0.238**	0.212	**0.183**	0.115	**0.327**	0.251	**0.251**	0.157
b-less		2	0.694	**0.226**	0.201	**0.174**	0.109	**0.333**	0.251	**0.251**	0.157

When FII_m/F_m at 760 nm is γ, and if we assume $FII_v/FII_m = F_v/F_m$ at 690 nm (no FI at 690 nm), then the two equations expressing F_m and F_v/F_m can be written:

$$FI_m + \gamma \cdot F_m = F_m$$

$$(1-\gamma) \cdot FI_v/FI_m + \gamma \cdot (F690_v/F690_m) = F760_v/F760_m$$

From these, the spillover ratio can be obtained as:

$$FI_\alpha = [1 - (F760_v/F760_m)/(F690_v/F690_m)] \cdot F760_m.$$

$$FI_\beta/FI_m = [(F760_v/F760_m)/(F690_v/F690_m) - \gamma]/(1-\gamma).$$

1152 Figures

1153

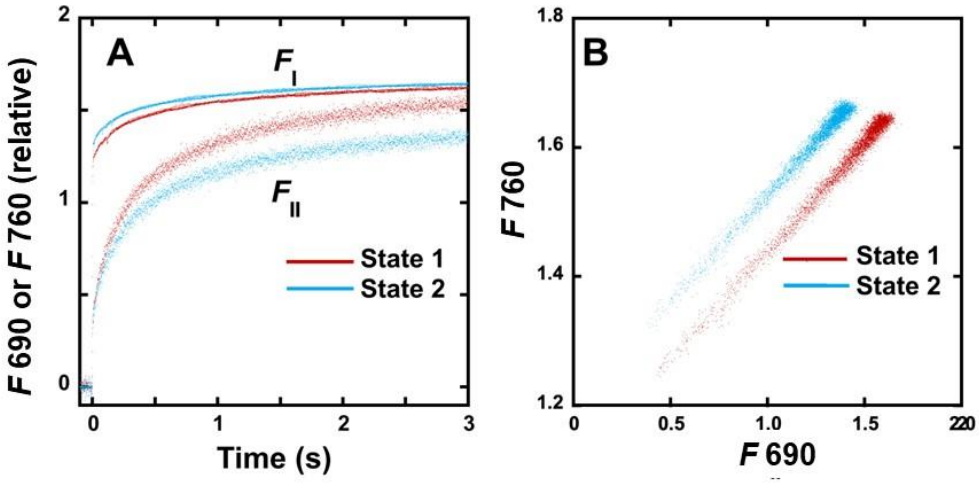

1154 Fig. 1. Induction curves of *F*690 and F760 and the relationships between *F*690 and
1155 *F*760 in LL- grown *A. odora*.

1156

1157 A, PSII fluorescence (*F*690) and mostly PSI fluorescence (*F*760) induction
1158 measured at 690 nm and 760 nm in leaf discs at 77K of LL- grown *A. odora*. Leaf
1159 discs were illuminated with PSI light at 720 nm inducing State 1 or PSII light at
1160 470 nm inducing State2, at the PFD of 5 μmol m^{-2} s^{-1}, for at least 30 min, kept in
1161 the dark for 1.5 to 2 min and frozen in liquid N_2. The fluorescence induction excited
1162 by the measuring/actinic light from a 460 nm LED pulse-modulated at 100 kHz was
1163 recorded. The PPFD level of the measuring/actinic light at the leaf disc was 50
1164 μmol m^{-2} s^{-1}. B, *F*760 plotted against *F*690.

1165

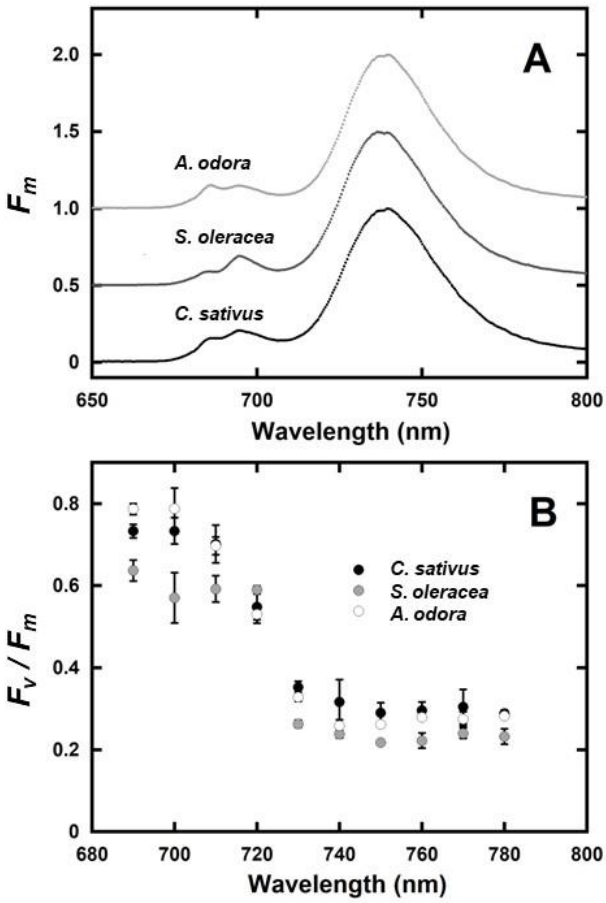

1166 Fig. 2. F_m spectra (A) and F_v/F_m spectra (B) for the wavelength range from 690 to
1167 780 nm in *C. sativus*, *S. oleracea* and *A. odora* leaf discs.
1168
1169 A, Emission spectra of F_m, excited by blue light from an LED peaked at 450 nm,
1170 were measured using a photodiode array spectrophotometer (C10083CAH,
1171 Hamamatsu Photonics, Japan). The F_m spectra were not corrected for the sensitivity
1172 of the photomultiplier. B, F_v/F_m in the leaf discs were measured using the band
1173 pass filters (Asahi-spectra). For both A and B, the leaf discs were treated in State
1174 1 light at 720 nm at 10 μmol m^{-2} s^{-1} at least for 30 min, kept in dim light or in the
1175 dark for 1.5 to 2 min, and frozen at 77K.
1176
1177

1178
1179
1180
1181

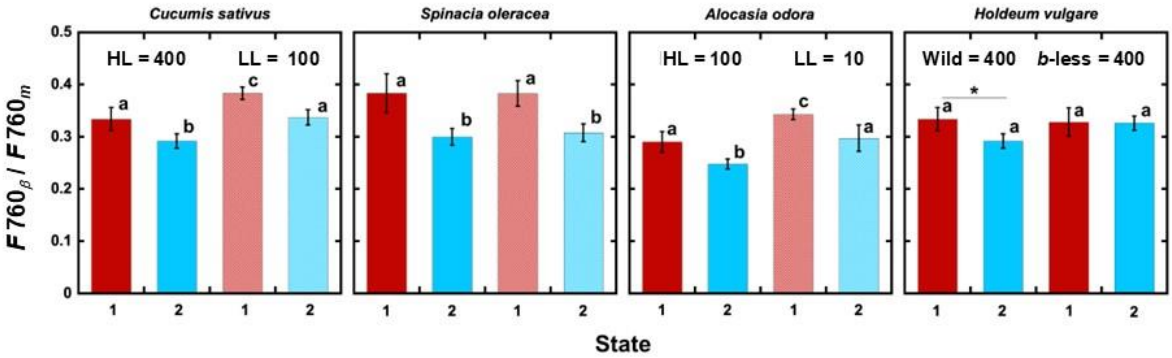

1182 Fig. 3. Spillover ratio ($F760_{\beta}/F760_{m}$) in leaf discs in the State 1 and State 2.
1183
1184 1 and 2 on the abscissa denote State 1 and State 2, induced by PSI and PSII light
1185 at 10 µmol m^{-2} s^{-1} at least for 30 min. For LL *A. odora*, PSI or PSII light was at 5
1186 µmol m^{-2} s^{-1}. HL and LL denote high and low growth light. 400, 100, and 10 denote
1187 growth PPFD levels in µmol m^{-2} s^{-1}. Different alphabets denote statistically
1188 significant differences ($P < 0.05$) by ANOVA (Tukey-Kramer test). For HL and LL
1189 *H. vulgare*, *t*-test was used (* denotes $P < 0.05$). For the data in this figure, no
1190 leftover FII_m at 760 nm was assumed. For the effects of the *F*II leftover, see Table
1191 3.
1192

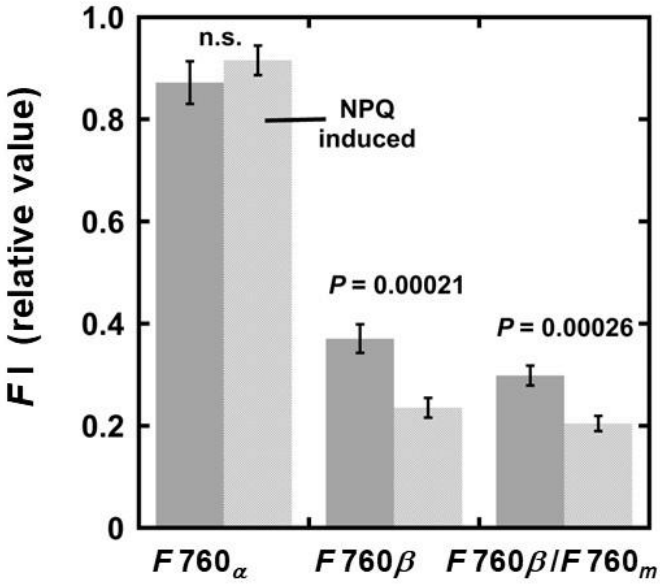

Fig. 4. Effects of NPQ induction on spillover of excitations from PSII to PSI in leaf discs from LL-grown *A. odora*.

Leaf discs from *A. odora* plants grown at 10 µmol m^{-2} s^{-1} were illuminated with a tungsten lamp at 700 µmol m^{-2} s^{-1} for 270 s and then illuminated with a 720 nm LED at 5 µmol m^{-2} s^{-1} for 10 s to oxidise the plastoquinone pool, and frozen. Inductions of *F*690 and *F*760 were measured. For the control, leaf discs treated in the dark and illuminated with the 720 nm LED at 5 µmol m^{-2} s^{-1} for 10 s were used. *P* values by *t*-test (n = 4) are shown. $F690_v$/ 690_m of the dark control and NPQ-induced samples were 0.81 ± 0.014 and 0.77 ± 0.009 (*P* = 0.00019, n = 4), while corresponding $F760_v$/ $F760_m$ were 0.24 ± 0.012 and 0.15 ± 0.010 (*P* = 0.00003, n=4).

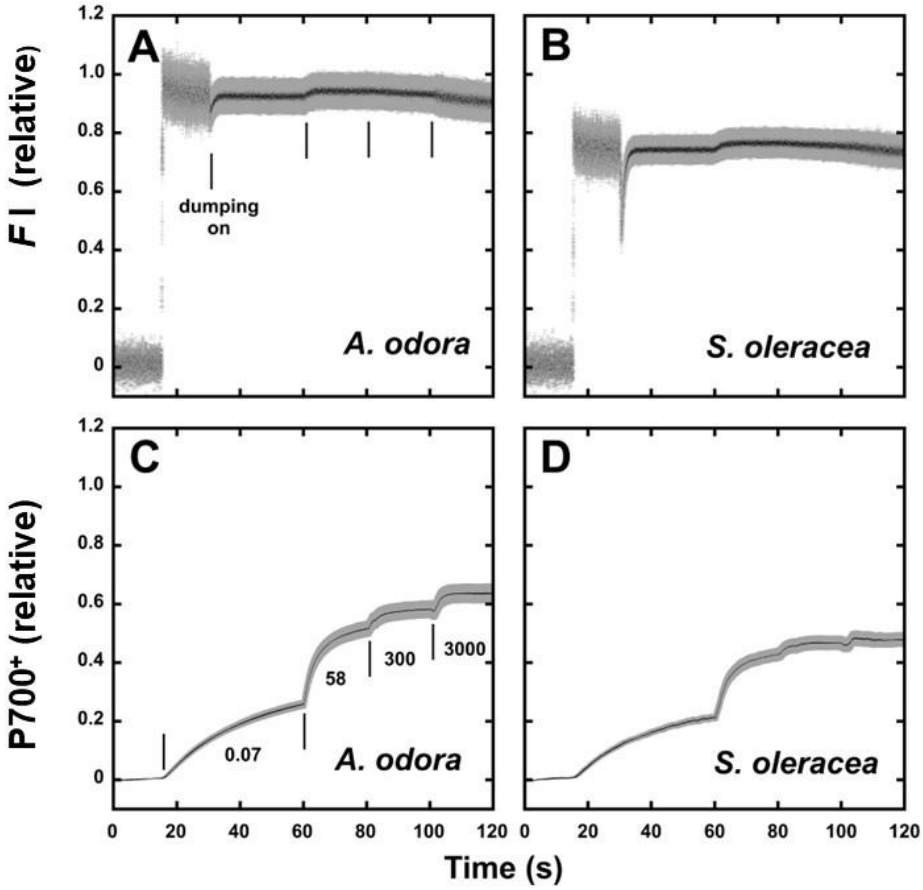

Fig. 5. PSI intrinsic fluorescence and $P700^+$ formation.

A and B, Induction of PSI intrinsic fluorescence excited at 700 nm and measured in the waveband > 730 nm in the leaf discs from LL-grn *A. odora* grown at 10 µmol m^{-2} s^{-1} (A) and from spinach grown at 400 µmol m^{-2} s^{-1} (B). C and D, Formation of $P700^+$ in response to 700 nm light at 0.07 µmol m^{-2} s^{-1}, 470 nm blue light at 58 and 360 µmol m^{-2} s^{-1}, and white incandescent light at 3000 µmol m^{-2} s^{-1}.

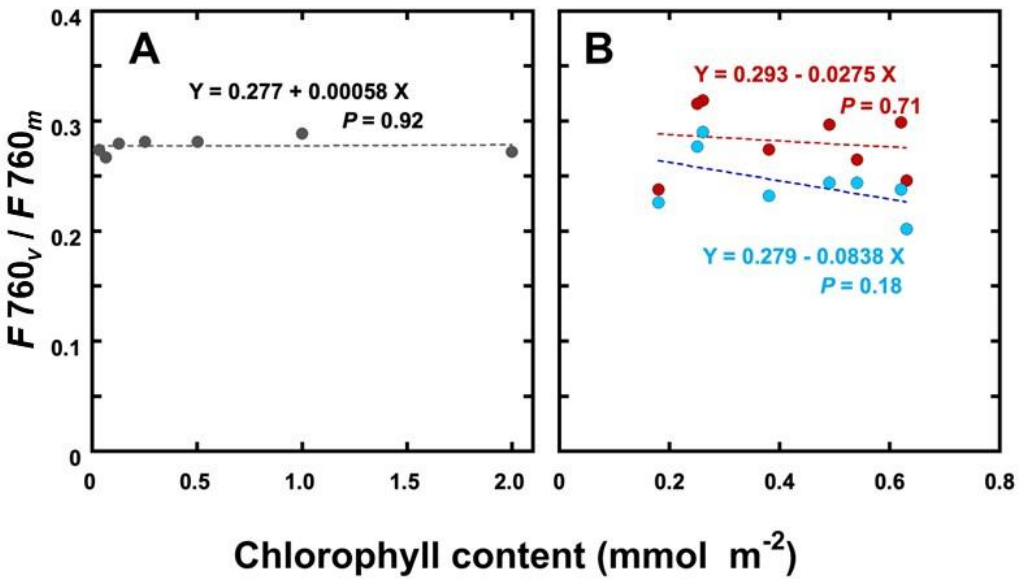

1217 Fig. 6. $F760_v/F760_m$ plotted against the chlorophyll concentration in the spinach
1218 thylakoid suspension (A) and in the leaf discs used for Fig. 3 (B).
1219
1220 A, Thylakoid suspensions were not pre-illuminated. The samples were kept in the
1221 dark before freezing. B, Symbols in red denote the data obtained in the State 1,
1222 while those in light blue denote the State 2. Equations are the linear regression
1223 lines. Neither of the slopes was statistically different from 0.
1224
1225

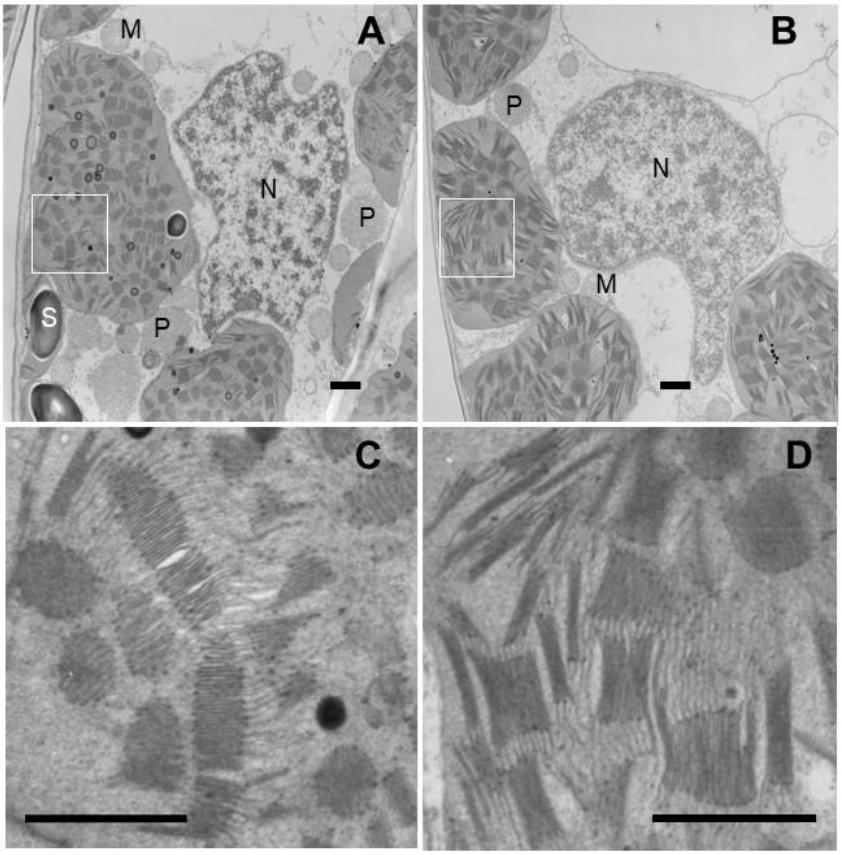

Fig. 7. Portions of the palisade tissue cells of *A. odora* leaves grown at high light (A and C) and low light (B and D).

For the electronmicroscopy study, the leaves grown at 180 and 10 μmol m^{-2} s^{-1} were used. SNear the well-developed chloroplasts, peroxisomes (P) and mitochondria (M) are observed in both samples (A and B). The square parts in A and B are enlarged in C and D. Starch grains (S) and lipid components (platoglobules) are more conspicuous in HL chloroplasts (A) than in LL chloroplasts (B). There are abundant non-appressed thylakoid membranes extending from grana stacks. Bars indicate 1 μm. The non-appressed thylakoid membranes / total thylakoid membranes in the central parts of these chloroplasts were 0.42 and 0.41 (See Figs. S9 and S10).

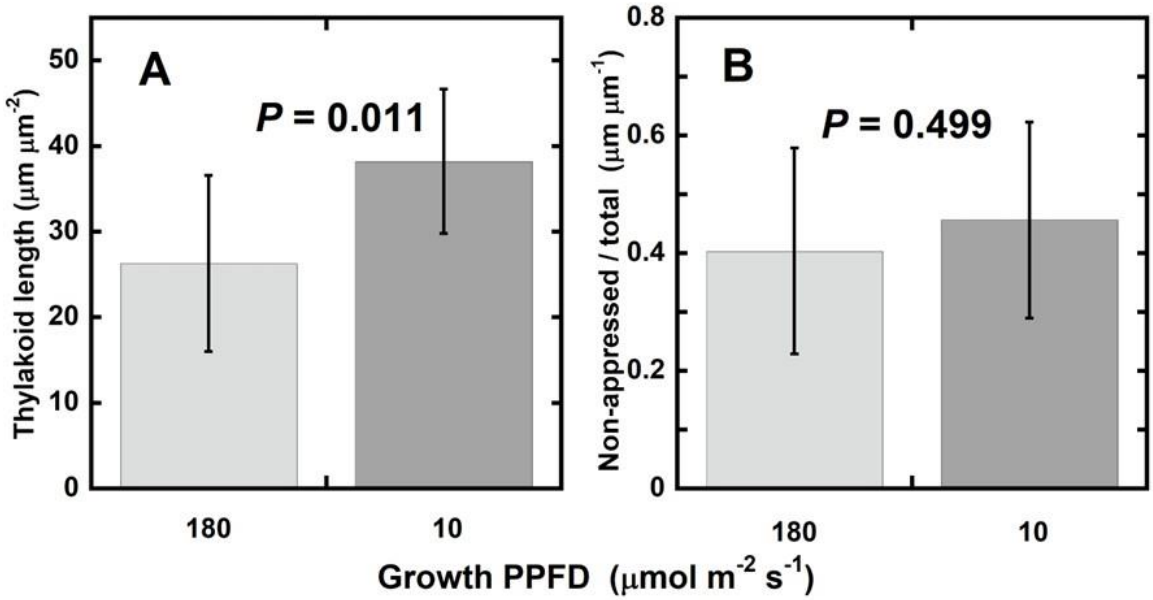

Fig. 8. Total length of thylakoid membranes per 1 μm^2 area (A) and the ratio of the total length of non-appressed thylakoid membranes to that of total thylakoid membranes (B).

On electron micrographs of chloroplasts, 1 μm^2 squares in which all the thylakoid membranes were in focus were chosen, and the morphometry data, total thylakoid membrane length (A) and the ratio of the total length of non-appressed thylakoid membranes to that of total thylakoid membranes (B) were obtained for leaf segments from an *A. odora* leaf grown at 180 $\mu mol\ m^{-2}\ s^{-1}$ and that grown at 10 $\mu mol\ m^{-2}\ s^{-1}$. The bar shows the mean for 10 squares (1 μm^2) from 10 different chloroplasts ± SD.

Supplementary materials

Table S1 *F*II induction time, $F690_m$, $F760_m$, and $F760_\alpha$

Table S2 Effects of the *F*II leftover at 760 nm on the fluorescence parameters shown in Fig. 4

Fig. S1. The optical system for the fluorescence measurement.

Fig. S2. Transmission spectra of the 690 and 760 nm band pass filters

Fig. S3. The relationship between F690 and F760 induction assuming no FII leftover at 760 nm.

Text 1: Estimation of the leftover *F*II at 760 nm (Fig. S4)

Text 2: Is *F*I excited by *F*II? (Figs. S5, 6, 7 and 8)

Figs. S9 and S10. Electron micrographs of *A. odora* chloroplasts showing how the ratios of non-appressed thylakoid membranes to the total length of thylakoids were measured.

Table S1. *F*II induction time, $F690_m$, $F760_m$, and $F760_\alpha$

	Growth light μmol m^{-2} s^{-1}	State	$t_{1/2}$ (s)	$F690_m$	$F760_m$	$F760_\alpha$
C. sativus	400	1	0.336 ± 0.017	1.58 ± 0.075 **	0.81 ± 0.074	0.51 ± 0.046
		2	0.344 ± 0.030	1.41 ± 0.027	0.94 ± 0.078 *	0.62 ± 0.054 +
	100	1	0.255 ± 0.017	1.73 ± 0.036 **	1.15 ± 0.053	0.71 ± 0.028
		2	0.279 ± 0.016 +	1.54 ± 0.079	1.18 ± 0.053	0.78 ± 0.050 *
S. oleracea	400	1	0.319 ± 0.055	1.49 ± 0.146 +	0.95 ± 0.135	0.59 ± 0.098
		2	0.338 ± 0.020	1.30 ± 0.082	1.08 ± 0.098	0.76 ± 0.063 *
	100	1	0.251 ± 0.023	2.15 ± 0.150 **	1.35 ± 0.103	0.83 ± 0.091
		2	0.307 ± 0.040 +	1.75 ± 0.076	1.30 ± 0.052	0.90 ± 0.055
A. odora	100	1	0.353 ± 0.013	1.40 ± 0.030 +	1.40 ± 0.077	1.00 ± 0.077
		2	0.377 ± 0.046	1.09 ± 0.056	1.36 ± 0.034	1.03 ± 0.030
	10	1	0.286 ± 0.026	1.68 ± 0.084 **	1.67 ± 0.071	1.10 ± 0.050
		2	0.326 ± 0.026 +	1.49 ± 0.082	1.69 ± 0.057	1.19 ± 0.045 *
H. vulgare WT	400	1	0.338 ± 0.029	1.54 ± 0.119 **	1.63 ± 0.058	1.09 ± 0.059
		2	0.493 ± 0.030 ***	1.30 ± 0.050	1.87 ± 0.075 **	1.32 ± 0.063 **
Chl *b*-less mutant	400	1	1.259 ± 0.080	0.41 ± 0.070	0.49 ± 0.092	0.33 ± 0.054
		2	1.348 ± 0.093	0.44 ± 0.062	0.51 ± 0.107	0.34 ± 0.079

+, *, **, and *** denote statistically significant differences between the data ($P < 0.1$, $P < 0.05$, $P < 0.01$ and $P < 0.001$ according to *t*-test) in State 1 and those in State 2.

The effects of growth light on $t_{1/2}$ are not compared statistically, because leaf materials per se were different. However, $t_{1/2}$ values were consistently smaller in low light grown materials.

We confined ourselves to compare the absolute fluorescence values in the samples from the same leaves, because optical properties were very different between HL and LL leaves even for the same species. Accumulation response of chloroplasts would occur in State 2 light (blue light at 10 or 5 μmol m^{-2} s^{-1}). This would increase $F\mathrm{II}_m$. But, in fact, $F\mathrm{II}_m$ decreased in State 2. Thus, the effect of chloroplast accumulation responses was weaker than that of the State transitions.

Table S2. Effects of the *F*II leftover at 760 nm on the fluorescence parameters shown in Fig. 4

		0%	5%	10%	20%
FI_v/FI_m	DARK	**0.241 ± 0.0120**	0.211	**0.178**	0.099
	NPQ	**0.152 ± 0.0100**	0.119	**0.083**	-
FI_m	DARK	**1.242 ± 0.0488**	1.180	**1.118**	0.994
	NPQ	**1.151 ± 0.0330**	1.093	**1.036**	-
FI_α	DARK	**0.872 ± 0.0361**	0.872	**0.872**	0.872
	NPQ	**0.915 ± 0.0249**	0.915	**0.915**	-
FI_β/FI_m	DARK	**0.298 ± 0.0196**	0.261	**0.220**	0.122
	NPQ	**0.204 ± 0.0149**	0.155	**0.160**	-

FI_α and FI_β/FI_m data at 0% leftover are shown in Fig. 5. When NPQ was developed, the assumption of 20% spillover resulted in a negative FI_v/FI_m value, indicating that the leftover was less than 20%. FI_v/FI_m becomes 0, when the leftover is 19.6%.

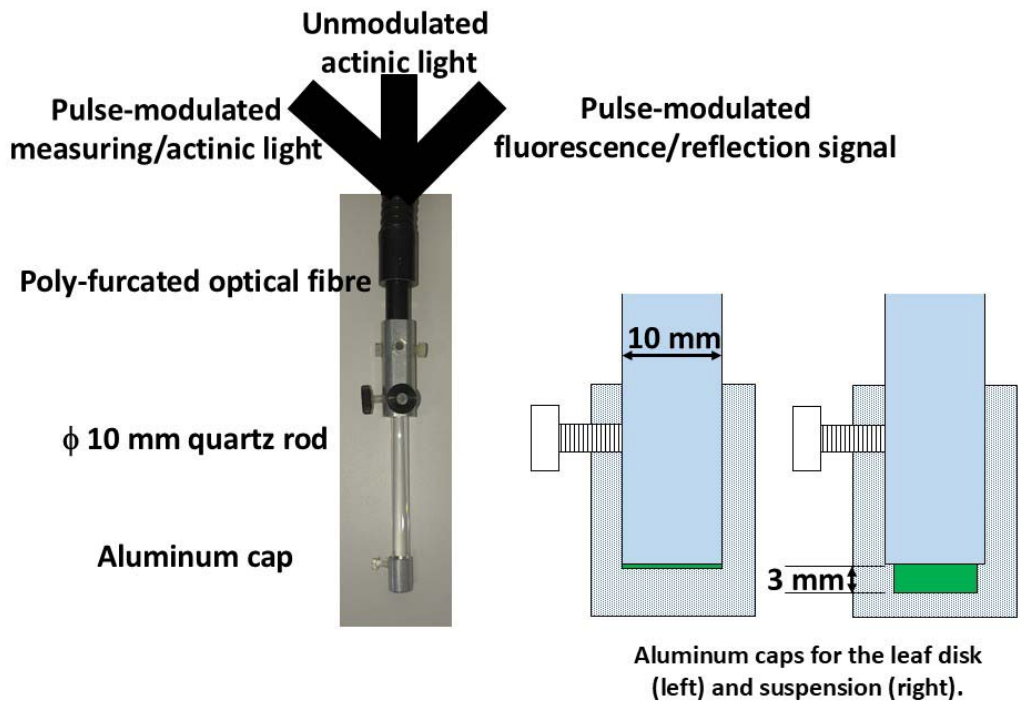

Fig. S1. The system for F_v/F measurement.

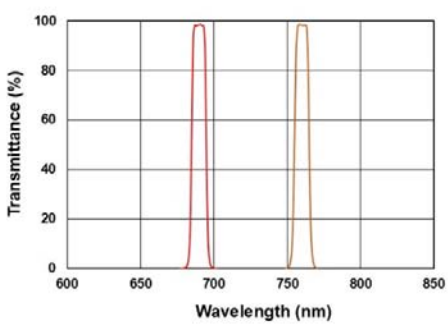

Fig. S2. Transmittance spectra of the 690 and 760 nm bandpass filters.
The half-band width was 10 nm. The tailings were small.

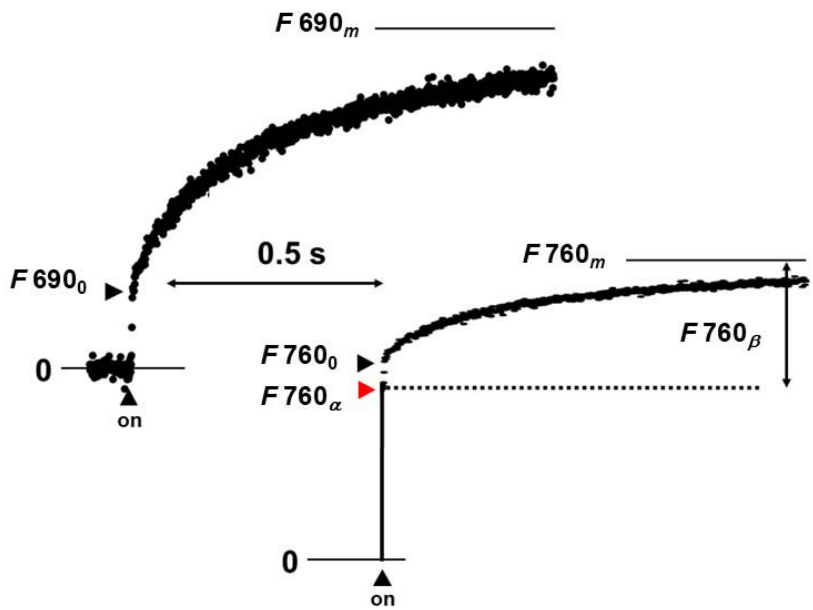

Fig. S3. Interrelationships between *F*690 and *F*760.

When the leftover PSII fluorescence at 760 nm is absent, induction of F760 is exclusively due to the spillover from PSII. However, if there is a leftover $F\mathrm{II}_m$ at 760 nm, we cannot distinguish the spillover from the contamination of *F*II.

When the leftover of $F\mathrm{II}_m$/ F_m at 760 nm was γ, and if we assume $F\mathrm{II}_v/F\mathrm{II}_m = F_v/F_m$ at 690 nm (no *F*I at 690 nm), two equations can be formulated :

$$F\mathrm{I}_m = (1-\gamma)\cdot F760_m$$
$$F\mathrm{I}_v/F\mathrm{I}_m = [F760_v/F760_m - \gamma\cdot(F690_v/F690_m)]/(1-\gamma)$$

From these, the $F\mathrm{I}_\alpha$ and the spillover ratio can be obtained as:

$$F\mathrm{I}_\alpha = [1-(F760_v/F760_m)/(F690_v/F690_m)]\cdot F760_m$$
$$F\mathrm{I}_\beta/F\mathrm{I}_m = [(F760_v/F760_m)/(F690_v/F690_m)-\gamma]/(1-\gamma)$$

Note that $F\mathrm{I}_\alpha$ is constant at any γ.

Estimation of the leftover *F*II at 760 nm

For this series of measurements, we grew *A. odora* and *C. sativus* outdoors in the soil in the pots. The *A. odora* plant used was the clone of the plants used in other measurements. For *C. sativus*, the same variety ('Nanshin') was used. We purchased *S. oleracea* from a local market. The measurements were conducted in July 2024, the warmest season.

Emission spectra of F_m, excited by blue light from an LED peaked at 450 nm, were measured using a photodiode array spectrophotometer (C10083CAH, Hamamatsu Photonics, Japan) and an optical system similar to that used for the F_v/F_m measurement as described in Terashima *et al*. (2021). F_v/F_m in the leaf discs were measured as described in detail in the Materials and Methods using the band pass filters. The leaf discs were treated in State 1 light at 720 nm at 10 μmol m^{-2} s^{-1} at least for 30 min. These spectra are shown in Fig. 2 in the main text.

We assumed that the $F\mathrm{II}_m$ would be expressed by a linear function for the wavelength range between 750 and 780 nm:

$$F\mathrm{II}_m(\lambda) = b - k(\lambda - 750) \qquad \text{Eq. S1}$$

where λ is wavelength in nm ($750 \leq \lambda \leq 780$). Then, the F_m level fluorescence at wavelength λ can be expressed as:

$$F\mathrm{I}_m(\lambda) + F\mathrm{II}_m(\lambda) = F\mathrm{I}_m(\lambda) + b - k(\lambda - 750) = \qquad \text{Eq. S2}$$

We assumed that $F\mathrm{II}_v/F\mathrm{II}_m$ was identical to that at 690 nm, $F690_v/F690_m$. Because $F\mathrm{I}_v/F\mathrm{I}_m$ is unknown, $F\lambda_v/F\lambda_m$ is expressed as:

$$\left(1 - \frac{b - k(\lambda - 750)}{F_m(\lambda)}\right) \cdot F\mathrm{I}_v/F\mathrm{I}_m + \frac{b - k(\lambda - 750)}{F_m(\lambda)} \cdot F690_v/F690_m = F\lambda_v/F\lambda_m \qquad \text{Eq. S3}$$

We obtained the set of b, k, $F\mathrm{I}_v/F\mathrm{I}_m$ that minimized the residual sum of squares (*RSS*) of the differences between the predicted and measured F_v/F_m values at four wavelengths:

$$RSS = \sum_{\lambda} \left[\left(1 - \frac{b - k(\lambda - 750)}{F_m(\lambda)}\right) \cdot \frac{F\mathrm{I}_v}{F\mathrm{I}_m} + \frac{b - k(\lambda - 750)}{F_m(\lambda)} \cdot \frac{F690_v}{F690_m} - \frac{F\lambda_v}{F\lambda_m}\right]^2 \qquad \text{Eq. S4}$$

The F_m spectra shown in Fig. 2 in the main text were not corrected for the sensitivity of the photomultiplier. However, we corrected the values using the data provided by the manufacturer (Hamamatsu photonics). Calculations were made with R statistical software (version 4.2.2; R Foundation

for Statistical Computing; available from http://www.R-proje ct.org). The function *nls* was used to obtain b, k and FI_v/FI_m by fitting nonlinear relationship among wavelength, F_m and F_v/F_m with the least-squares method. We measured three F_v/F_m values for each wavelength for each species. The three independent variables were estimated using all these values. For *S. oleracea* and *A. odora*, FI_v/FI_m significantly significant values were obtained, whereas for *C. sativus*, the value was not statistically supported probably due to scattering of the FI_v/FI_m values. When the mean F_v/F_m value for each wavelength was used, a statistically significant FI_v/FI_m was obtained (Table 3 in the main text). Fitting of these models to the measured values are shown in Fig. S4. When statistically significant values were used, the changes in F_v/F_m with λ were well traced.

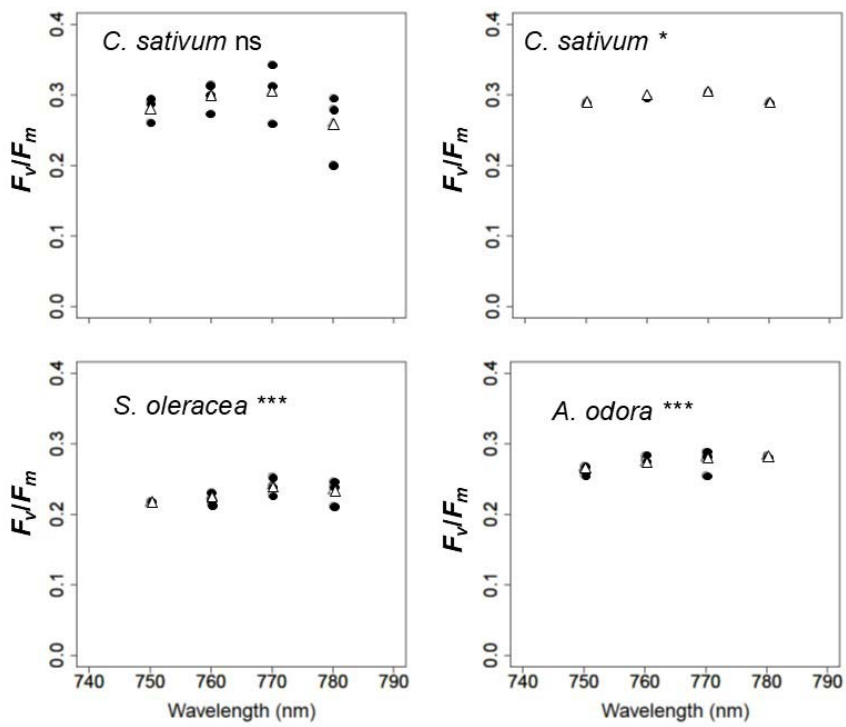

Fig. S4. The data used for the fitting and the modelled values.

Open circles were the raw data or mean values of the raw data. Solid triangles were modelled F_v/F_m values.

* and *** denote that FI_v/FI_m determined were statistically significant at $P< 0.05$ and $P< 0.001$.

Is *F*I excited by *F*II?

Using a simple model (Fig. S5), we calculate light absorbed by a thin layer, emission of PSII fluorescence by this layer, re-absorption of this fluorescence by the rest of the leaf, and emission of PSI fluorescence caused by the absorption of PSII fluorescence, in this order. Then, the ratio of the *F*I excited by *F*II to the *F*I directly driven by the blue light will be calculated.

Transmission of the monochromatic light through a pigment solution in a cuvette is expressed by the Lambert-Beer's law:

$$-\log_{10}\frac{I_t}{I_0} = \varepsilon \cdot c \cdot l \qquad \text{Eq. S5}$$

where I_0 and I_t are intensities of the incident light and transmitted light, l is the cuvette thickness, ε is an absorption coefficient, and c is the pigment concentration. Here, we consider the cumulative pigment concentration C in mol m^{-2}:

$$C = c \cdot l \qquad \text{Eq. S6}$$

Using a simple model, let us compare PSI fluorescence directly excited by the actinic light and that excited by PS II fluorescence (see Fig. S5).

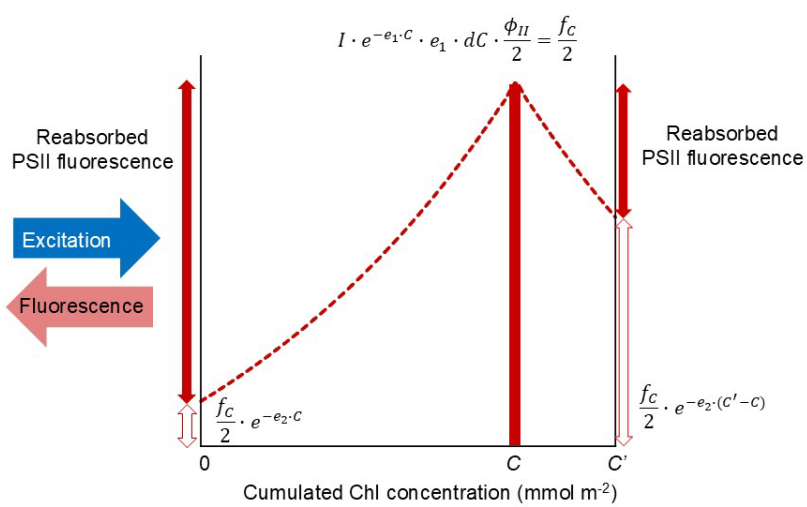

Fig. S5. A model leaf used for estimation of PSI fluorescence excited by re-absorbed PSII fluorescence.

A thin leaf layer dC absorbs light and emits fluorescence. The fluorescence emitted by dC is expressed as f_C for simplicity.

Let us consider a thin layer (*dC*) at the cumulated chlorophyll concentration of *C* from the illuminated surface. Light absorption by this thin layer (*dA*) can be written as:

$$dA = I \cdot e^{-e_1 C} \cdot e_1 \cdot dC \qquad \text{Eq. S7}$$

where e_1 is equal to $2.30 \cdot \varepsilon_1$ and ε_1 is the absorption coefficient of Chl *a*+*b* at 460 nm (in $m^2\ mol^{-1}$). Note that $\log_e 10 = 2.30$. PSII fluorescence emitted by this thin layer can be expressed as:

$$dF\mathrm{II} = \phi_{\mathrm{II}} \cdot I \cdot e^{-e_1 \cdot C} \cdot e_1 \cdot dC \qquad \text{Eq. S8}$$

where ϕ_{II} denote PSII fluorescence yield.

Since PSII fluorescence emitted by a thin layer *dC* is absorbed by both sides of the layer, PSII fluorescence re-absorbed in a leaf or solution ($0 < X < C'$) can be expressed as:

$$dA = I \cdot e^{-e_1 \cdot C} \cdot e_1 \cdot dC \cdot \frac{\phi_{\mathrm{II}}}{2} \cdot \left[\left(1 - e^{-e_2 \cdot C}\right) + \left(1 - e^{-e_2 \cdot (C' - C)}\right)\right] \qquad \text{Eq. S9}$$

where e_2 $(= 2.30 \cdot \varepsilon_2)$ and ε_2 *is* the absorption coefficient of Chl *a*+*b* at PSII fluorescence peak (~690 nm). PSI fluorescence excited by PSII fluorescence would not be re-absorbed. Then, PSI fluorescence from *dC* excited by PSII fluorescence and detected at the surface would be half the PSI fluorescence:

$$dF\mathrm{I}_{\leftarrow F\mathrm{II}} = I \cdot e^{-e_1 \cdot C} \cdot e_1 \cdot dC \cdot \frac{\phi_{\mathrm{II}}}{2} \cdot \frac{\phi_{\mathrm{I}}'}{2} \cdot \left[\left(1 - e^{-e_2 \cdot C}\right) + \left(1 - e^{-e_2 \cdot (C' - C)}\right)\right] \qquad \text{Eq. S10}$$

where ϕ_{I}' denotes the yield of PSI fluorescence excited by PSII fluorescence. On the other hand, PSI fluorescence directly excited by the actinic light, emitted by the thin layer at *C* (*dC*), and detected by the sensor is expressed as:

$$dF\mathrm{I}_{direct} = \frac{\phi_{\mathrm{I}}}{2} \cdot I \cdot e^{-e_1 \cdot C} \cdot e_1 \cdot dC \qquad \text{Eq. S11}$$

where ϕ_{I} denotes the yield of PSI fluorescence excited by the blue actinic light. Integration from 0 to C' of these equations give:

$$F\mathrm{I}_{\leftarrow F\mathrm{II}} = \frac{\phi_{\mathrm{II}}}{2} \cdot \frac{\phi_{\mathrm{I}}'}{2} \int_0^{C'} I \cdot e^{-e_1 \cdot C} \cdot e_1 \cdot \left[\left(1 - e^{-e_2 \cdot C}\right) + \left(1 - e^{-e_2 \cdot (C' - C)}\right)\right] dC \qquad \text{Eq. S12}$$

$$F\mathrm{I}_{direct} = \frac{\phi_{\mathrm{I}}}{2} \int_0^{C'} I \cdot e^{-e_1 \cdot C} \cdot e_1 \cdot dC = \frac{\phi_{\mathrm{I}}}{2} \cdot I \cdot \left(1 - e^{-e_1 \cdot C'}\right) \qquad \text{Eq. S13}$$

The ratio of these integrals is expressed as:

$$\frac{F_{\mathrm{I}\leftarrow F_{\mathrm{II}}}}{F_{\mathrm{I}\,direct}} = \frac{\phi_{\mathrm{II}}}{2} \cdot \frac{\phi_{\mathrm{I}}'}{\phi_{\mathrm{I}}} \cdot \frac{\int_0^{C'} I \cdot e^{-e_1 \cdot C} \cdot e_1 \cdot \left[\left(1-e^{-e_2 \cdot C}\right)+\left(1-e^{-e_2 \cdot (C'-C)}\right)\right] dC}{\int_0^{C'} I \cdot e^{-e_1 \cdot C} \cdot e_1 \cdot dC} \qquad \text{Eq. S14}$$

Because we may neglect the effects of PSII fluorescence emitted to the other side, PSII fluorescence emitted from dC and reaches the surface can be expressed as:

$$dF\mathrm{II}_{surface} = \frac{\phi_{\mathrm{II}}}{2} \cdot I \cdot e^{-e_1 \cdot C} \cdot e_1 \cdot dC \cdot e^{-e_2 \cdot C} = \frac{\phi_{\mathrm{II}}}{2} \cdot I \cdot e^{-(e_1+e_2) \cdot C} \cdot e_1 \cdot dC$$

Eq. S15

The absorption coefficients *in situ*, e_1 and e_2, may be estimated by examining the effects of the cumulated Chl concentration of the thylakoid suspension on PSI and PSII fluorescence.

PSII fluorescence reaching the surface can be estimated by integrating Eq. S15:

$$\frac{\phi_{\mathrm{II}}}{2} \cdot I \int_0^{C'} e_1 \cdot e^{-(e_1+e_2) \cdot C} \cdot dC = \frac{\phi_{\mathrm{II}}}{2} \cdot I \cdot \frac{e_1}{(e_1+e_2)} \cdot \left(1 - e^{-(e_1+e_2) \cdot C'}\right) \qquad \text{Eq. S16}$$

By curve fitting of the dependence of PSI and PSII fluorescence (Eqs. S13 and S16) on C', e_1 and e_2 may be estimated (see Fig. S6 for the estimation of e_1).

The ratio (Eq. S14) is a function of PSII and PSI fluorescence yields and absorption coefficients. The ratio increases with C' (Fig. S9). Since PSII fluorescence little excites PSII fluorescence while preferentially excites PSI, ϕ_{I}' would be twice of ϕ_{I}. Then, Eq. A10 may become:

$$\frac{F_{\mathrm{I}\leftarrow F_{\mathrm{II}}}}{F_{\mathrm{I}\,direct}} \approx \phi_{\mathrm{II}} \cdot \frac{\int_0^{C'} I \cdot e^{-e_1 \cdot C} \cdot e_1 \cdot \left[\left(1-e^{-e_2 \cdot C}\right)+\left(1-e^{-e_2 \cdot (C'-C)}\right)\right] dC}{\int_0^{C'} I \cdot e^{-e_1 \cdot C} \cdot e_1 \cdot dC} \qquad \text{Eq. S17}$$

Hence, ϕ_{II} is the key factor. The ratio of the integrals in the realistic C' range is at most 1~2 (Fig. S9). Because PSII fluorescence yield excited by blue light, ϕ_{II}, is small (Latimer et al. 1956, Lamb et al. 2018 and references therein), the effects of PSII fluorescence re-absorption on PSI fluorescence should be also small.

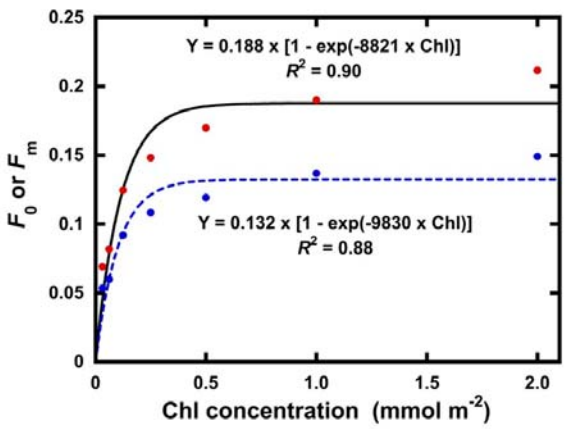

Fig. S6. Determination of e_1. In this calculation, we assume that no PSI fluorescence is excited by PSII fluorescence.

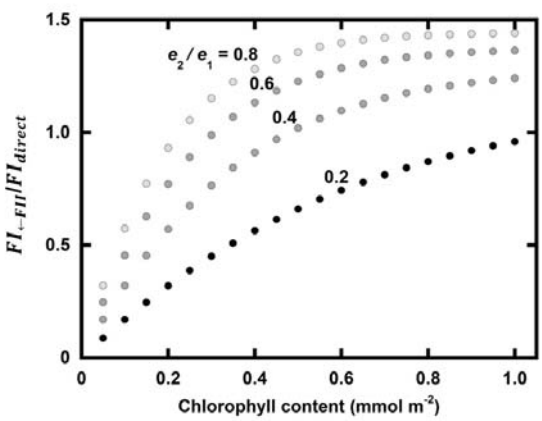

Fig. S7. The ratio of the integrations in Eq. S17:

$$\frac{\int_0^{C'} I \cdot e_1 \cdot e^{-e_1 \cdot C} \cdot [(1 - e^{-e_2 \cdot C}) + (1 - e^{-e_2 \cdot (C' - C)})] dC}{\int_0^{C'} I \cdot e_1 \cdot e^{-e_1 \cdot C} \cdot dC}$$

The ratio increases with the increase in C'. For e_1, we used 9000 (namely ε_1 of 9000/2.3 = 3913 m^2 mol^{-1}, see Fig. S6). We did not estimate e_2 experimentally. Several possible e_2 values were used (see Fig. S8).

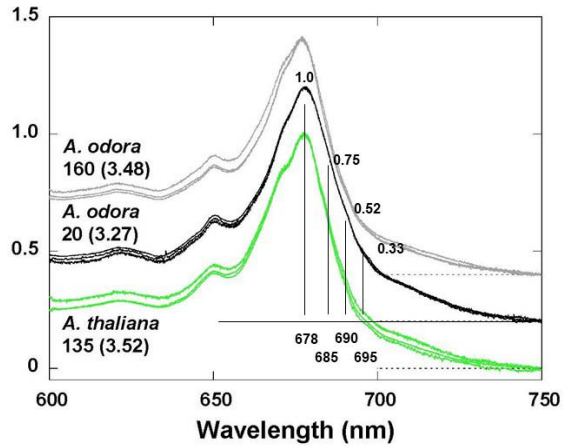

Fig. S8. 77K absorbance spectra of thylakoid suspensions prepared from the leaves of *A. odora* grown at 160 and 20, and *Arabidopsis thaliana* grown at 135 µmol m^{-2} s^{-1}. Assuming the red peak (678 nm) height is similar to that at 460 nm, e_2 at 685, 690 and 695 nm were estimated for low light *A. odora*. The original figure in Terashima et al. (2021) was modified.

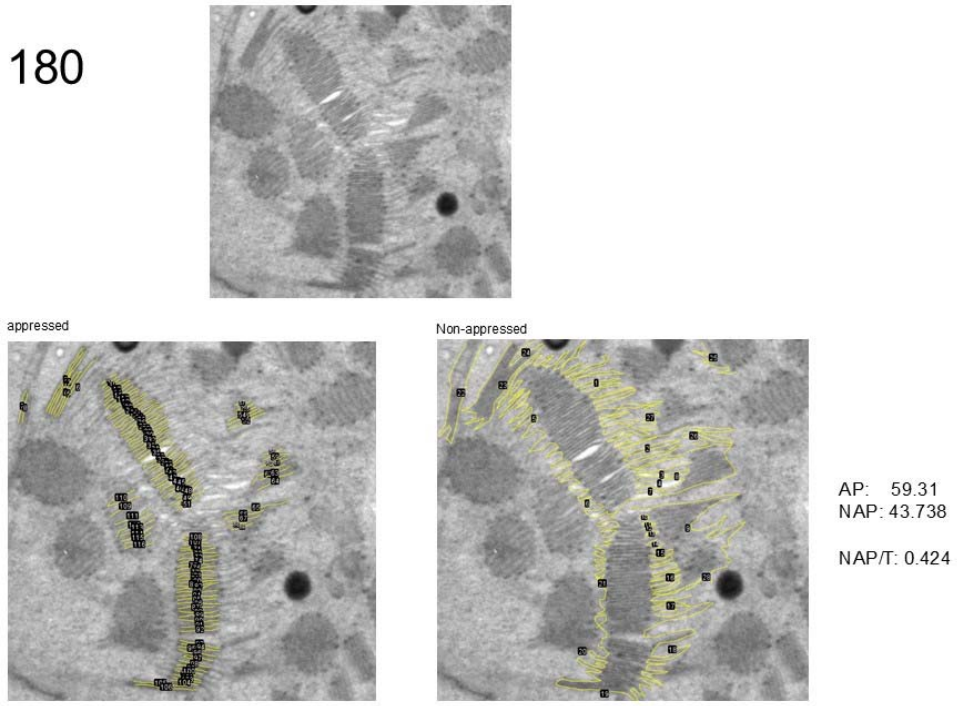

Fig. S9. A part of a HL-*A. odora* chloroplast.

Determination of the length of non-appressed thylakoid membranes (NAP) and appressed thylakoid membranes (AP). The ratio of NAP to the total length (NAP+AP) was 0.424.

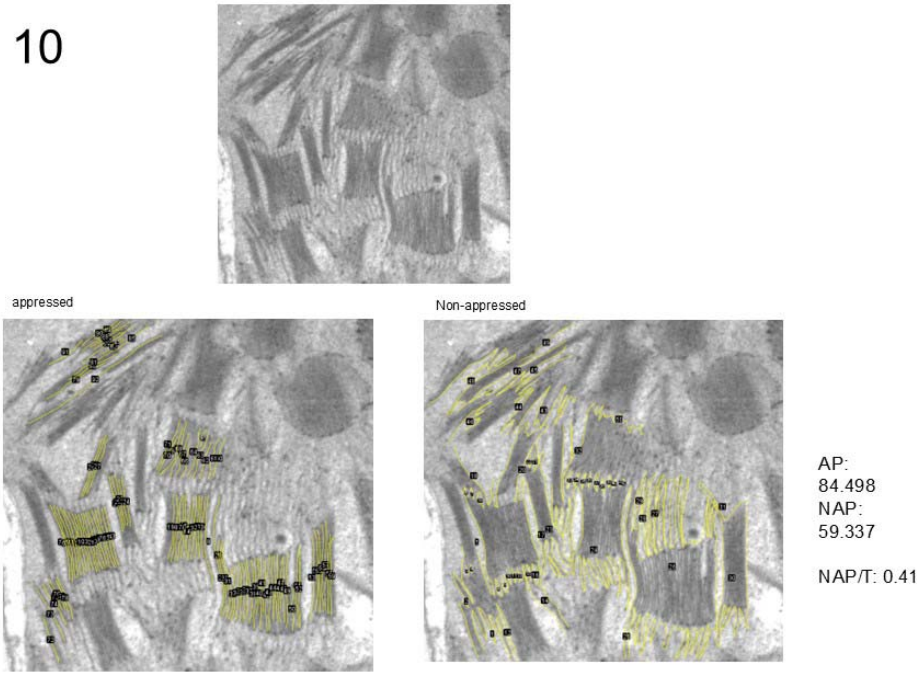

Fig. S10. A part of a HL-*A. odora* chloroplast.

Determination of the length of non-appressed thylakoid membranes (NAP) and appressed thylakoid membranes (AP). The ratio of NAP to the total length (NAP+AP) was 0.41.